Hydroschorlomite in altered basalts from Hole 1256D, ODP Leg 206: The transition from low-temperature to hydrothermal alteration

Christine Laverne, Olivier Grauby, Jeffrey C. Alt, Marcel Bohn

Hydroschorlomite in altered basalts from Hole 1256D, ODP Leg 206: The transition from low-temperature to hydrothermal alteration

Christine Laverne

Laboratoire de Pétrologie Magmatique, Case 441, Université Paul Cézanne Aix–Marseille III, Faculté des Sciences et Techniques, Avenue Escadrille Normandie–Niemen, F-13397 Marseille Cedex 20, France (christine.laverne@univ-cezanne.fr)

Olivier Grauby

CRMCN-CNRS, Campus de Luminy, Case 913, F-13288 Marseille Cedex, France

Jeffrey C. Alt

Department of Geological Sciences, University of Michigan, Ann Arbor, Michigan 48109-1005, USA

Marcel Bohn

IFREMER–Centre de Brest, CNRS-UMR 6538, Technopole Brest–Iroise, BP 70, F-29280 Plouzané, France

[1] Hydroschorlomite, a Ti-, Ca-, Fe-rich andraditic garnet present in the deepest cores of basalts (661–749 mbsf) drilled in Hole 1256D during Ocean Drilling Program (ODP) Leg 206 (equatorial east Pacific), is reported here for the first time in oceanic crust. Detailed petrological and mineralogical studies by optical microscope, electron microprobe, scanning and transmission electron microscope, and micro-Raman spectroscopy are used to characterize this hydrogarnet and its relationships with other minerals. Hydroschorlomite occurs in Hole 1256D as small ($5–50$ μm) anhedral or euhedral crystals associated either with celadonite in black halos adjacent to celadonite veins or with brown saponitic phyllosilicate in brown alteration halos adjacent to veins of saponite and iron oxyhydroxides. Both types of halos are formed at low temperature (less than about 100°C). Textural observations suggest that hydroschorlomite formation is contemporaneous with the phyllosilicates. Hydroschorlomite is rich in CaO (22.5–26.5 wt%), TiO$_2$ (22.0–28.6 wt%), and FeO$_t$ (6.2–12.9 wt%) and contains significant F (up to 0.85 wt%) and Zr$_2$O$_3$ (up to 0.34 wt%). The presence of OH suggested by the low total percentages of oxides (95.2–97.3 wt%) is confirmed by the OH vibration at 3557 cm^{-1} in the micro-Raman spectrum. Chemical mapping indicates that hydroschorlomite is not zoned and is always associated with either celadonitic or saponitic phyllosilicates. Some hydroschorlomite crystals partly include tiny (<10 μm) skeletal titanomagnetite. The occurrence of hydroschorlomite in Hole 1256D basalts coincides with a general downward increase in temperatures and overall intensity of alteration manifest by the alteration of plagioclase and the occurrence of small amounts of mixed-layer chlorite-smectite. The titanium necessary to form hydroschorlomite is provided by the breakdown of primary tiny (<10 μm) titanomagnetite, while calcium is provided by the replacement of plagioclase by albite. Hydroschorlomite is thus an indicator of alteration of titanomagnetite under conditions transitional from low-temperature alteration to hydrothermal metamorphism with formation of titanite and may affect magnetic properties of the rocks.

————————————————

Theme: Formation and Evolution of Oceanic Crust Formed at Fast Spreading Rates
Guest Editors: Damon A. H. Teagle and Doug Wilson

1. Introduction

[2] Garnet is common in oceanic crust that has been subducted and subjected to high-pressure metamorphism, but it is rare in in situ oceanic crust. Hydrogarnet is present in oceanic metagabbros associated with serpentinized peridotites [e.g., *Honnorez and Kirst*, 1975]. *Laverne* [1983] describes a unique occurrence of melanite in a single vein from basalt from DSDP/ODP Hole 504B, interpreted as having formed from deuteric and Ca-rich hydrothermal fluids at temperatures of 300–400°C during cooling of the lava.

[3] Hydroschorlomite, a hydrated Ti-, Ca-, Fe-andradititic garnet, has been discovered in association with green celadonitic and orange-brown saponitic phyllosilicate in the deepest cores of basalts ((661–749 meters below the seafloor (mbsf)) recovered in Ocean Drilling Program (ODP) Hole 1256D during Leg 206. The purpose of this paper is to describe this newly discovered occurrence of hydrogarnet, to document its chemical composition and crystal chemistry, and to discuss its conditions of formation and its relation to the general alteration of Hole 1256D basalts. We suggest that hydroschorlomite is an indicator of alteration conditions transitional from low-temperature to hydrothermal metamorphism, and that hydroschorlomite may affect magnetic properties of the rocks.

2. Geological Background

[4] Hole 1256D (6°44.2′N, 91°56.1′W) is located in the Guatemala basin, on the eastern flank of the East Pacific Rise (Figure 1) [*Shipboard Scientific Party*, 2003]. It lies within ∼15 Ma oceanic lithosphere of the Cocos plate accreted at a superfast spreading rate (∼200–220 mm/yr [*Wilson*, 1996]). On ODP Leg 206 Hole 1256D was cored to 749

mbsf, or 502 m into basaltic basement, composed of sheet flows, pillow lavas, hyaloclastites, massive lava flows and rare dikes.

[5] The recovered basalts experienced variable low-temperature alteration processes [*Shipboard Scientific Party*, 2003]. A pervasive dark gray background alteration characterized by the presence of small amounts of saponite results from interaction with seawater at low temperatures and low water/rock ratios. Different colored alteration halos are developed adjacent to veins and fractures. Dark green or black halos, characterized by the presence of celadonite, are interpreted as resulting from interaction with upwelling low-temperature hydrothermal fluids possibly mixed with seawater (see summary by *Alt* [2004]). Brown, red and orange oxidization halos are formed later by interaction of the basalt with cold, oxidizing seawater, and similar effects occur superimposed on dark halos, resulting in "mixed" halos. This vein-related alteration occurs irregularly throughout Hole 1256D but is concentrated in two zones, at 350–450 and 635–749 mbsf [*Shipboard Scientific Party*, 2003]. The deeper of these two intervals includes the depth interval where hydroshorlomite occurs (Figure 2).

3. Analytical Procedures

[6] Electron microprobe analyses of primary and secondary minerals and chemical mapping were carried out at IFREMER (Brest, France) on a Cameca SX50 using the ZAF correction program [*Pouchou and Pichoir*, 1985]. Operating conditions were (1) for spot analyses −15 kV accelerating voltage, 15 nA beam current, 1 μm spot size, 6 s counting time and (2) for chemical mapping −15 kV accelerating voltage, 40 nA specimen current, 512 × 512 points each 2 microns, 140 ms per point.
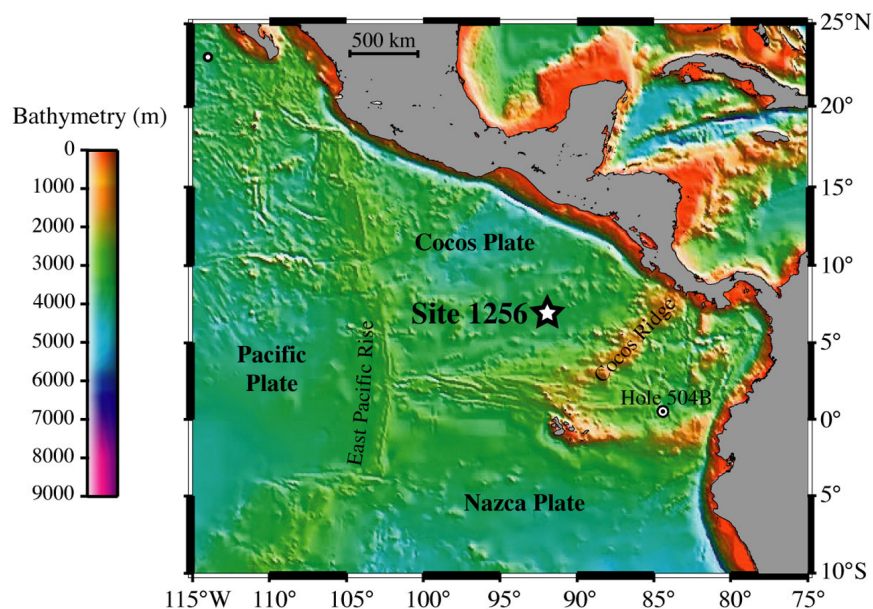
Figure 1. Bathymetric map showing the location of ODP Site 1256 in the Cocos Plate (modified after *Shipboard Scientific Party* [2003]). Location of DSDP/ODP Hole 504B is shown for comparison.

[7] SEM imaging was performed on a JEOL 6320 FEG scanning electron microscope at the CRMCN (Marseille, France). Semi-quantitative chemical analyses during SEM observations were performed using Energy Dispersive X-ray Spectrometry (EDS).

[8] A micro-Raman spectrum was recorded with a 1 cm^{-1} spectral resolution using a Renishaw inVia system equipped with a Spectra Physics Ar+ Laser (514.5 nm, 20 mW) (CICRP, Marseille, France). A Leica DMLM microscope with a $50\times$ NPLAN objective and a 10x multiplying lens was used to focus the laser beam on the thin section. Resultant interaction areas correspond to circular spots of 1.8 μm in diameter. Raman photons from a limited depth interval were collected by using a confocal hole. The spectrum was recorded over the [100–3800] cm^{-1} range using a Notch filter. Photons were collected using a Peltier cooled charge-coupled device (CCD) detector. Calibration was performed using the 520.5 cm^{-1} of a silicon wafer. The spectrum was the result of 120 during 60-s acquisitions, with an effective power of 0.12 mW.

[9] Cross-sectioning for TEM analysis by the focused ion beam (FIB) milling technique was performed with a FEI Model 200 TEM FIB system at the University Paul Cézanne Aix-Marseille III. The FIB lift-out method was used as described by *Heaney et al.* [2001]. The same area as that observed by SEM was located using the imaging
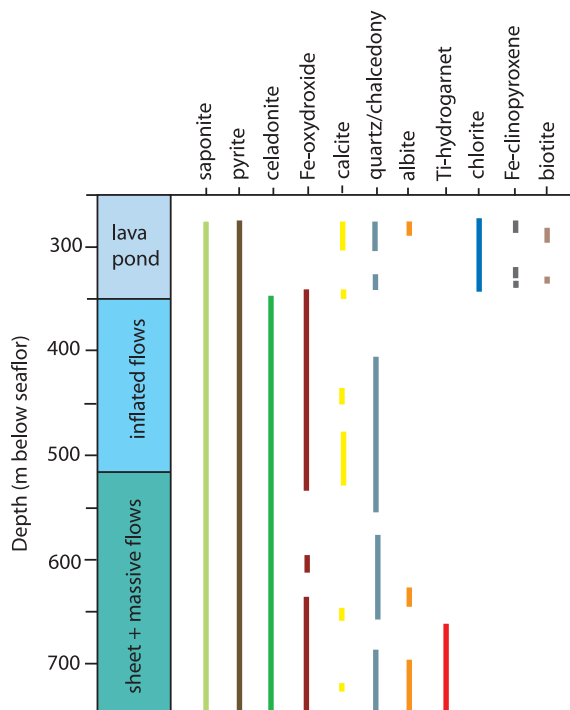
Figure 2. The distribution of hydroschlormite is shown schematically in the context of the distribution of all secondary minerals in Hole 1256D (modified after *Shipboard Scientific Party* [2003]). The distribution of secondary clinopyroxene is after *Shipboard Scientific Party* [2003] and C. Laverne (unpublished data, 2005).

Table 1. Petrographic Features of the Hydroschorlomite-Bearing Samples and Nearby Samples From Hole 1256D, ODP Leg 206[a]

Hole	Core Section	Interval, cm	Depth, mbsf	Vein or Vug Mineralogical Composition	Hydsch.-Bearing Rock Type	Hydsch. Ass. Mineral	Plagioclase Replacement	Hydsch. Abund.
1256D	59R-2	131–135	661.68	Fe-oxhydr, sm, sm/cel	khaki halo	cel	no	((x))
1256D	60R-1	70–73	669.30	sm/cel, sm, pyr	khaki brwn halo	cel	no	((x))
1256D	61R-1	139–143	679.39	cel, (sm)	khaki brwn halo	cel	brwn sm core (sec F rim?)	(x)
1256D	62R-1	23–26	687.43	no	dk grn halo + brwn halo	cel	brwn sm + sec F	x
1256D	63R-1	50–53	697,00	sm, chalc	khaki brwn halo	cel	sec F	x
1256D	63R-1	81–83	697.31	no	-	-	ab, chalc	no
1256D	64R-2	41–44	702.96	Fe-oxhydr, chalc, sm/cel	khaki halo	cel	brwn sm	x
1256D	65R-1	105–109	706.75	Fe-oxhydr	brwn halo	cel	brwn sm	x
1256D	65R-3	27–31	708.79	Fe-oxhydr, chalc	-	-	brwn sm core + sec F rim	no
1256D	66R-1	14–17	710.54	Fe-oxhydr, (cel), sm	host rock	cel	brwn sm + sec F	x
1256D	67R-1	47–50	715.27	Fe-oxhydr, cel, (chalc)	dk grn halo	cel	brwn sm core + ab rim	x
1256D	67R-2	85–90	717.09	sm, chalc	khaki halo	cel	brwn sm + sec F core	x
1256D	67R-3	5–8	717.72	Fe-oxhydr, cel, chalc	khaki brwn halo	cel	brwn sm core (sec F rim?)	x
1256D	68R-1	100–102	720.50	sm, chalc	host rock	cel, sap	brwn sm + sec F	x
1256D	68R-1	113–117	720.63	cel, hydsch??, chalc, (sm)	host rock	cel, sap	brwn sm + sec F	x
1256D	69R-1	73–76	724.83	cel/sm, (cel), op, chalc	orange halo	cel	brwn sm + ?	x
1256D	70R-2	8–12	730.24	Fe-oxhydr?	host rock	cel	Fe-oxhydr	x
1256D	71R-1	95–99	734.25	cel, chalc	host rock	cel	sec F	x
1256D	72R-1	111–115	739.01	cel, chalc, hydsch?	khaki halo	cel	?	x
1256D	72R-2	84–88	740.24	chalc	host rock	sap	Fe-oxhydr	(x)
1256D	73R-1	75–78	743.15	chalc, (cel, hydsch?)	host rock	cel	?	(x)
1256D	74R-1	111–112	748.31	no	-	-	ab, sm	no
1256D	74R-2	81–85	749.35	chalc, Fe-oxhydr	orange halo + host rock	sap	Fe-oxhydr	x

[a] Column 4: sample depth in meters below seafloor. Column 5: minerals within veins or vugs (in italics). Fe-oxhydr, iron oxyhydroxide; sm, smectite; sm/cel, smectite/celadonite mixture; pyr, pyrite; chalc, chalcedony; hydsch, hydroschorlomite. Minerals in parentheses are minor phases. Column 6: hydroschorlomite-bearing rock type; brwn, brown; dk gm, dark green. Column 7: minerals associated with hydroschorlomite. Column 8: minerals replacing plagioclase; sm, smectite; sec F, secondary feldspar (when the occurrence of albite has not been checked by microprobe; ab, albite (checked by microprobe). "Host rock" refers both to a clearly identified host rock adjacent to an alteration halo and to a homogeneous sample that is probably a dark green alteration halo. Column 9: occurrence and abundance of hydroschorlomite; x, common; (x), uncommon; ((x)), rare; no, none.
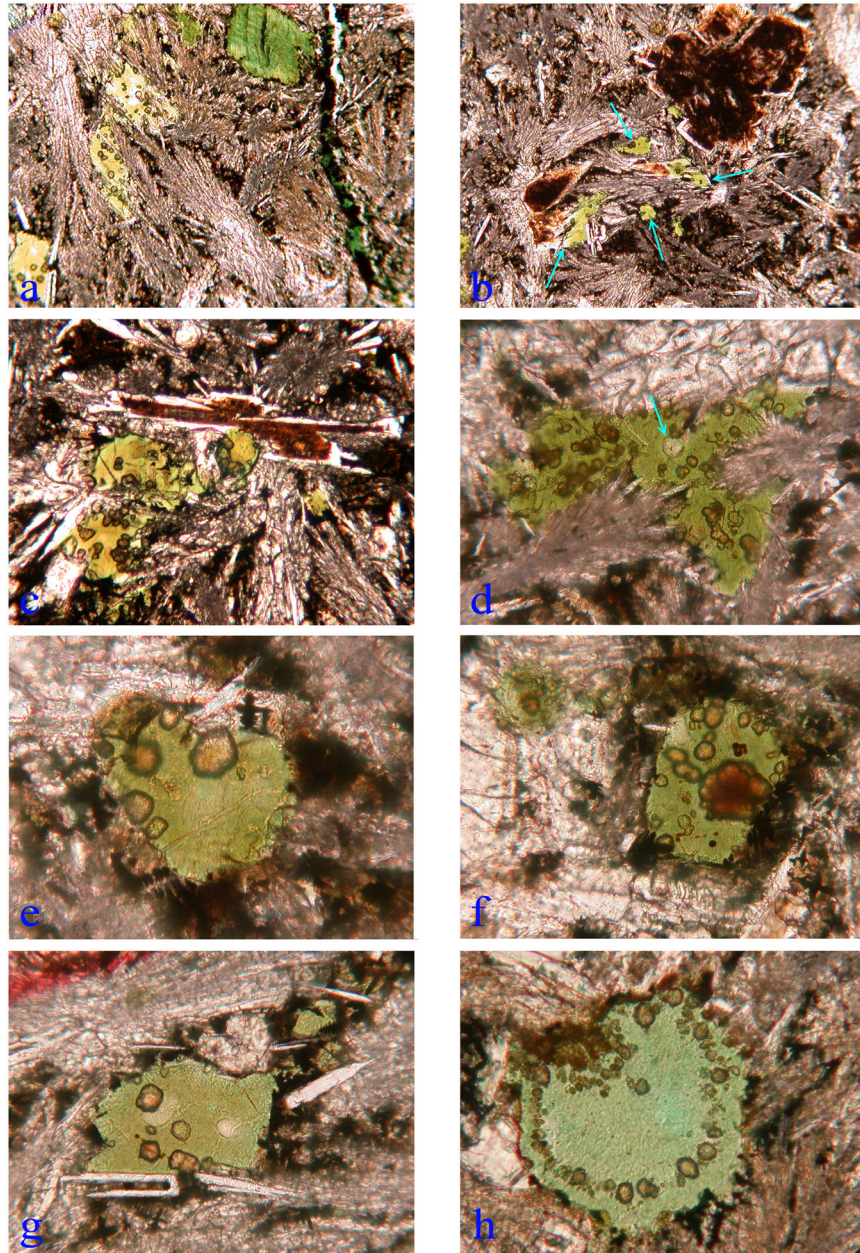
Figure 3

capabilities of the FIB. A thin layer of platinum was then deposited on the specimen surface to protect the hydroschorlomite during the milling process. The FIB system uses a Ga liquid metal ion source for milling. A 30 kV Ga^{2+} beam operating at ∼20 nA excavated hydroschorlomite from both sides of the Pt layer to a depth of 5 μm, resulting in a thin cross section. Before removal of the thin section, the sample was further thinned to an electron-transparent thickness of ∼80nm using a glancing angle beam at much lower beam currents of ∼100 pA. Finally, a line pattern was drawn with the ion beam along the side and bottom edges of the thin section, allowing its removal. The ∼15 μm × ∼5 μm × 80nm slide was transferred at room pressure with the aid of a stereomicroscope and a hydraulic micromanipulator. A glass needle was positioned close to the thin slide, which was then electrostatically attracted to the needle. The foil was then placed onto the membrane of a carbon-coated 200-mesh copper grid.

[10] TEM studies were carried out at CRMCN of Marseille using a JEOL-3010, operated at an accelerating potential of 300 kV. Microanalyses were acquired with a JEOL-2000FX operating with an accelerating potential of 200 kV with a Si (Li) detector fitted with a UTW and a TRACOR Northern 5500 EDS system. In fixed transmission mode, the spot size diameter ranged from 100 to 40 nm. Quantitative data were obtained by the method developed by *Cliff and Lorimer* [1975] after calibration of the $k_{x,Si}$ factors (x = Al, Mg, . . .) against natural and synthetic layer silicates of known and homogeneous composition.

4. Descriptions and Chemical Compositions

4.1. Optical Microscope

[11] In the deepest basalts (661–749 mbsf) from Hole 1256D (Table 1), hydrogarnet occurs as a minor phase associated with (1) celadonite filling vesicles and miarolitic voids of the dark green, khaki, or black alteration halos (Figure 3) [*Laverne*, 2006] or (2) orange-brown phyllosilicate occurring in interstitial areas and as vesicle fillings of orange oxidized and mixed alteration halos (Figure 4) (see detailed description of a hydroschorlomite-bearing mixed halo from Hole 1256D by *Busigny et al.* [2005]). Hydrogarnet crystals (generally 5 to 20 μm in diameter, but up to 50 μm) are ovoid in shape with irregular boundaries or less commonly euhedral (Figures 3e and 3g). They are very pale brown, have high relief, and are slightly anisotropic. They occur either as isolated crystals (e.g., Figure 3e) or as clusters of several coalescing crystals (e.g., Figure 3f), as confirmed by SEM study. Their location in vesicles and miarolitic voids varies: they may lie at the edge or in the central part of these features (Figures 3d, 3e, 3f, and 3g), or, in one case, as small crystals making a ring within celadonite (Figure 3h), suggesting that these two minerals can be contemporaneous.

Figure 3. Photomicrographs of hydroschorlomite associated with celadonite in Hole 1256D basalts (plane parallel light). (a) Vein composed of celadonite (dark green) where it crosses magmatic plagioclase and iron-oxyhydroxides (very dark brown) where it cuts magmatic clinopyroxene. In the dark green alteration halo adjacent to this vein, olivine close to the vein is completely replaced by K_2O-rich (7.9–8.9 wt%) dark green celadonite, whereas K_2O poorer (5.3–6.3 wt%) yellow-green celadonite, associated with hydroschorlomite, fills pore spaces and replaces olivine further from the vein (Sample 206-1256D-65R-1,105–109 cm; field of view: 1 mm). (b) In dark green alteration halo, plagioclase phenocrysts and microphenocrysts are extensively replaced by dark brown saponite ± iron-oxyhydroxides, and only a thin external rim is unaltered or locally replaced by albite. Interstitial areas and vesicles are filled with green celadonite and hydroschorlomite (arrows) (Sample 206-1256D-65R-1,105–109 cm; field of view 800 μm). (c) Same as Figure 3b, in Sample 206-1256D-66R-1, 14–17 cm; field of view 700 μm). (d) Miarolitic void filled with yellow green celadonite and hydroschorlomite. Note the abundance of the hydroschorlomite crystals (pale brown, high relief) and the presence of one slightly larger silica mineral globule (colorless, arrow). The plumose or feather-like aggregates are magmatic clinopyroxene crystals (Sample 206-1256D-65R-1,105–109 cm; field of view 450 μm). (e) Detail of a vesicle filled with yellow green celadonite and subhedral or euhedral hydroschorlomite. Note the hexagonal section of the largest hydroschorlomite crystal and note the presence of skeletal titanomagnetite adjacent to the vesicle (Sample 206-1256D-65R-1, 105–109 cm; field of view 250 μm). (f) Detail of a vesicle filled with yellow green celadonite and subhedral hydroschorlomite. Note that the central part of the aggregate of hydroschorlomite crystals is composed of orange brown iron-hydroxides. The diffuse boundaries of some of the hydroschorlomite crystals indicate they are below the surface of the thin section (Sample 206-1256D-65R-1, 105–109 cm; field of view 300 μm). (g) Yellow green celadonite and subhedral hydroschorlomite probably replacing a euhedral olivine microphenocryst (Sample 206-1256D-65R-1, 105–109 cm; field of view 350 μm). (h) Vesicle filled with bluish green celadonite and hydroschorlomite. Note the distribution of hydroschorlomite as a ring within celadonite (Sample 206-1256D-63R-1, 50–53 cm; field of view 320 μm).
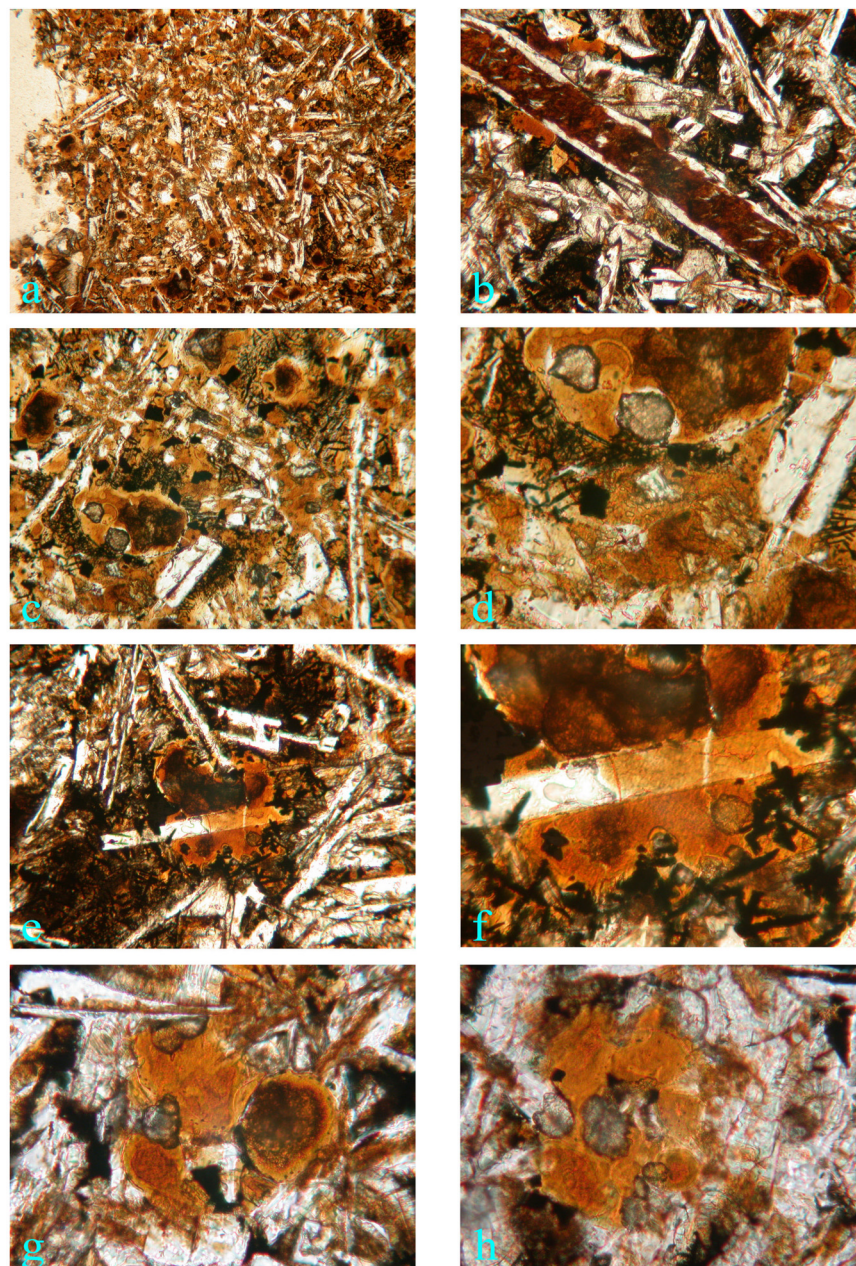
Figure 4. Photomicrographs of hydroschorlomite associated with orange brown saponite in Sample 206-1256D-74R-2, 81–85 cm (plane parallel light). (a) General view of the oxidized brown alteration halo (2 mm thick) adjacent to a vug filled with chalcedony (colorless, at left). Note that primary clinopyroxene and olivine are completely (and plagioclase is partly) replaced by brown saponite (field of view 1.5 mm). (b) In the host rock adjacent to the oxidized halo, the center of a plagioclase microphenocryst is replaced by brown saponite (Table A2), whereas its outer rim is fresh (Table A5). Note that clinopyroxene is slightly altered (field of view 600 μm). (c) Vesicle filled with orange brown saponite and hydroschorlomite in oxidized alteration halo (field of view 600 μm). (d) Detail of Figure 4c. Note that the diameter of hydroschorlomite crystals can reach 50 μm in this sample, and note the population of very fine grained titanomagnetite (field of view 250 μm). (e) Coalescing vesicles; same caption as Figures 4c and 4d (field of view 600 μm). (f) Detail of Figure 4e (field of view 250 μm). (g and h) Probable subhedral olivine microcrystals replaced by orange brown saponite and hydroschorlomite (field of view 250 μm).

[12] Minor chalcedony globules, similar in size or slightly larger than the hydrogarnets, commonly occur in celadonite-hydroschorlomite-bearing voids and vesicles (Figure 3d). Very small skeletal titanomagnetite crystals are commonly in contact with these vesicles and voids (e.g., Figures 3e and 3h). In dark green alteration halos, magmatic clinopyroxene is generally fresh, whereas primary
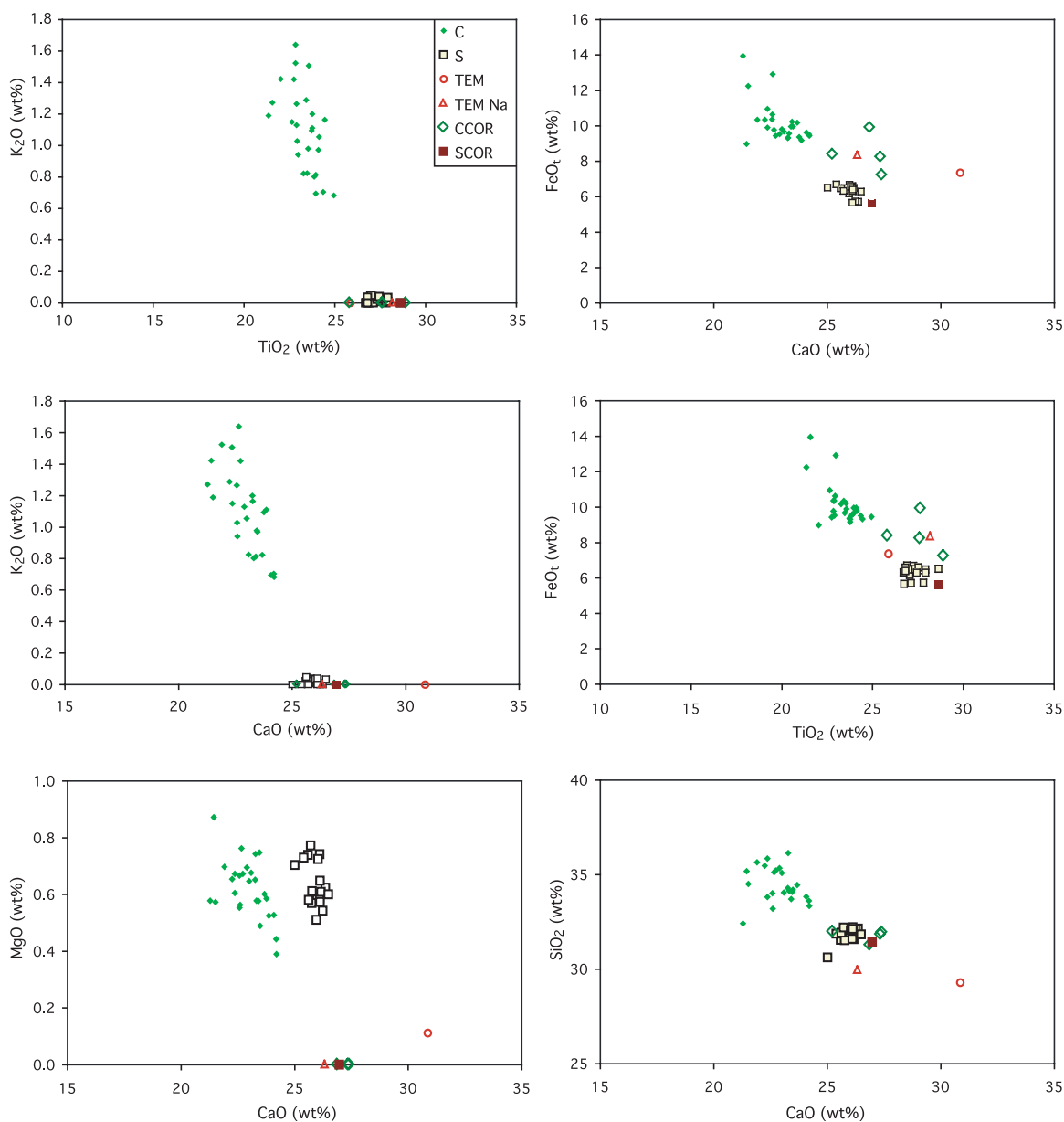
Figure 5. Plot of oxide contents of hydroschorlomite obtained by EMP and TEM. C, hydroschorlomite associated with celadonite (EMP analyses, Table A1); S, hydroschorlomite associated with saponite (EMP analyses, Table A1); CCOR, hydroschorlomite corrected for the presence of celadonite inclusions (see text for explanation); SCOR, hydroschorlomite corrected for the presence of saponite inclusions; TEM, end-member hydroschorlomite composition determined by TEM and corrected for celadonite inclusions (no Na analysis) (see text for explanation, Figure 16, and Table A7). Analysis recalculated assuming 5 wt% H_2O; TEM (Na), same as previous but including analysis of Na.

plagioclase phenocrysts are completely, or less commonly partly, replaced by brown saponite and/or albite (Figures 3b and 3c). In some of the more highly oxidized orange alteration halos (e.g., Sample 206-1256D-74R-2, 81–86 cm), saponite completely replaces clinopyroxene and partly replaces plagioclase (Figure 4b).

4.2. Electron Microprobe

4.2.1. Hydroschorlomite

[13] Electron microprobe analyses (Table A1) reveal that this garnet is rich in CaO (22.5–26.5 wt%), TiO_2 (22.0–28.6 wt%), and FeO_t (6.2–12.9 wt%), and the low total percentages of oxides (95.2–97.3 wt%)
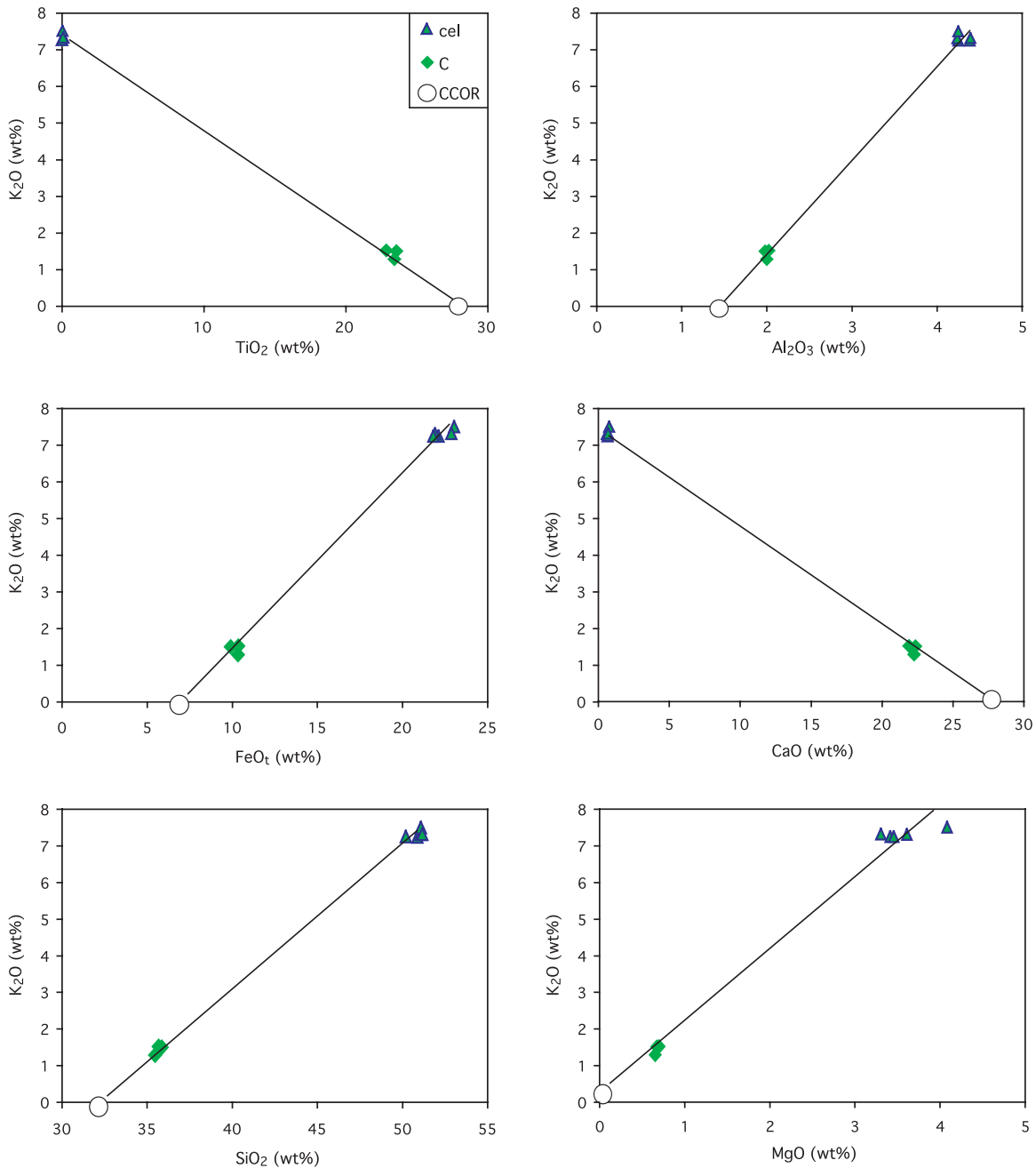
Figure 6. Example of determination of the hydroschorlomite end-member (CCOR) from EMP analyses of celadonite (cel) and hydroschorlomite (C) containing celadonite inclusions in a single vesicle of Sample 1256D-67R-1, 47–54 cm (see text for explanation).

suggest the presence of OH. Note that FeO_t represents all Fe as FeO but the oxidation state of Fe is discussed in section 5.1. Significant F (up to 0.85 wt%) and Zr_2O_3 (up to 0.34 wt%) are present whereas Cl and Y_2O_3 contents are insignificant.

[14] While the name melanite is used for varieties of titanian andradite garnet that have $Fe^{3+} > Ti$ in the octahedral position, those with $Fe^{3+} < Ti$ are called schorlomite [*Huggins et al.*, 1977a, 1977b; *Deer et al.*, 1982]. This division is close to the 15 percent TiO_2 boundary originally proposed by *Zedlitz* [1933]. Given the high TiO_2 contents and the presence of OH in Hole 1256D schorlomite (see section 4.5), it is referred to as hydroschorlomite in the present paper. The hydroschorlomite crystals in Hole 1256D are chemically homogeneous and unzoned. The crystals in a given sample

Table 2. Comparison of Compositions of Hydroschorlomite From Hole 1256D, ODP Leg 206[a]

End-member	EMP	EMP	EMP	EMP	EMP	TEM	TEM Na
Association	cel ass	cel ass	cel ass	cel ass	sap ass	cel ass	cel ass
Hole	1256D	1256D	1256D	1256D	1256D	1256D	1256D
Core section	65R-1	65R-1	65R-1	67R-1	74R-2	70R-2	70R-2
Interval, cm	105−109	105−109	105−109	47−54	81−85	8−12	8−12
SiO_2	31.98	31.84	31.28	31.95	31.44	30.83	31.51
TiO_2	25.82	27.61	27.65	28.92	28.62	27.23	29.67
Al_2O_3	1.79	1.15	1.12	1.44	2.27	1.59	0.83
CaO	25.23	27.35	26.88	27.41	26.98	32.48	27.73
Na_2O	0.00	0.00	0.06	0.06	0.08	nd	1.48
K_2O	0.00	0.00	0.00	0.00	0.00	0.00	0.00
FeO	8.38	8.24	9.91	7.23	5.59	7.74	8.78
MgO	0.42	0.00	0.00	0.00	nd	0.12	nd
Total	93.62	96.20	97.04	97.01	94.99	100.00	100.00

[a] Compositions are in weight percent. Columns 1−4: calculated EMP end-members of hydroschorlomite associated with celadonite (see text for explanation). Column 5: calculated EMP end-member of hydroschorlomite associated with saponite. Columns 6 and 7: calculated TEM end-members of hydroschorlomite associated with celadonite without Na_2O data (column 6) and with Na_2O data (column 7) (see text for explanation). All Fe and Ti are considered as FeO and TiO_2, respectively. nd, not determined.

show only slight chemical variations but there is greater variation from one sample to another.

[15] Two apparent compositional groups can be distinguished and are correlated with the associated mineral assemblage (Table A1, Figure 5). In Cores 63R through 67R, hydrogarnet is associated with celadonite, and the electron microprobe (EMP) analyses have higher Si, Fe, and K contents than analyses of hydrogarnet from Core 74R, where it is associated with saponite. These analytical variations thus reflect the presence of inclusions or intergrowths of phyllosilicate within the garnets, as revealed by SEM, TEM and micro-Raman analyses (see sections 4.4 through 4.6).

4.2.2. Associated Minerals

[16] Dark green celadonite from the hydroschorlomite-bearing samples is particularly K_2O-rich, whereas a yellow-green "celadonitic mineral" is poorer in K_2O and FeO_t and more hydrated, suggesting a celadonite/smectite mixture (Table A3; Figure 3a). Dark orange brown iron-oxyhydroxides (Table A4) occur in veins of most of the celadonite-bearing samples. The composition of the iron oxyhydroxides is fairly constant (FeO_t: 70.2–73.8 wt%) and includes some SiO_2 (about 5 wt%). In the celadonite-free samples, the orange-brown phyllosilicate occurring in vesicles and interstitial areas and as replacement of plagioclase cores (Table A2) is relatively Al-rich. This is within the compositional range of other saponitic phyllosilicates from Hole 1256D [*Alt and Laverne*, 2006] and other oceanic basalts, however, and has been termed Al-saponite [e.g., *Alt*, 1999]. Table A5

presents chemical analyses of primary plagioclase and secondary albite that commonly replaces plagioclase phenocrysts and rims of microphenocrysts. Due to the small size of titanomagnetite crystals, we could obtain only one acceptable analysis (Table A6).

4.2.3. Corrected Hydroschorlomite Analyses

[17] In order to correct the EMP analyses for the celadonite inclusions while taking into account the variability of celadonite compositions, we assume that in a given vesicle, celadonite included within hydroschorlomite has the same composition as celadonite external to the garnet. For a given vesicle, we plot all oxides versus K_2O for both hydroschorlomite and celadonite (see example in Figure 6). Because each EMP analysis of hydroschorlomite is a binary mixture of K-bearing celadonite and hydrogarnet that is assumed to be K-free, the trend of EMP analyses projected to 0% K_2O provides an estimate of the end-member hydrogarnet composition. The individual analyses of hydroschorlomite, labeled "C" for "celadonite-associated hydroschorlomite" project to this end-member composition, labeled "CCOR" for "celadonite associated corrected hydroschorlomite" (Figure 6). Four EMP end-members were determined in this way from four different vesicles. These end-members have higher CaO and TiO_2 contents and lower FeO_t than the analyses of hydroschorlomite-celadonite mixtures (Table 2, Figure 5).
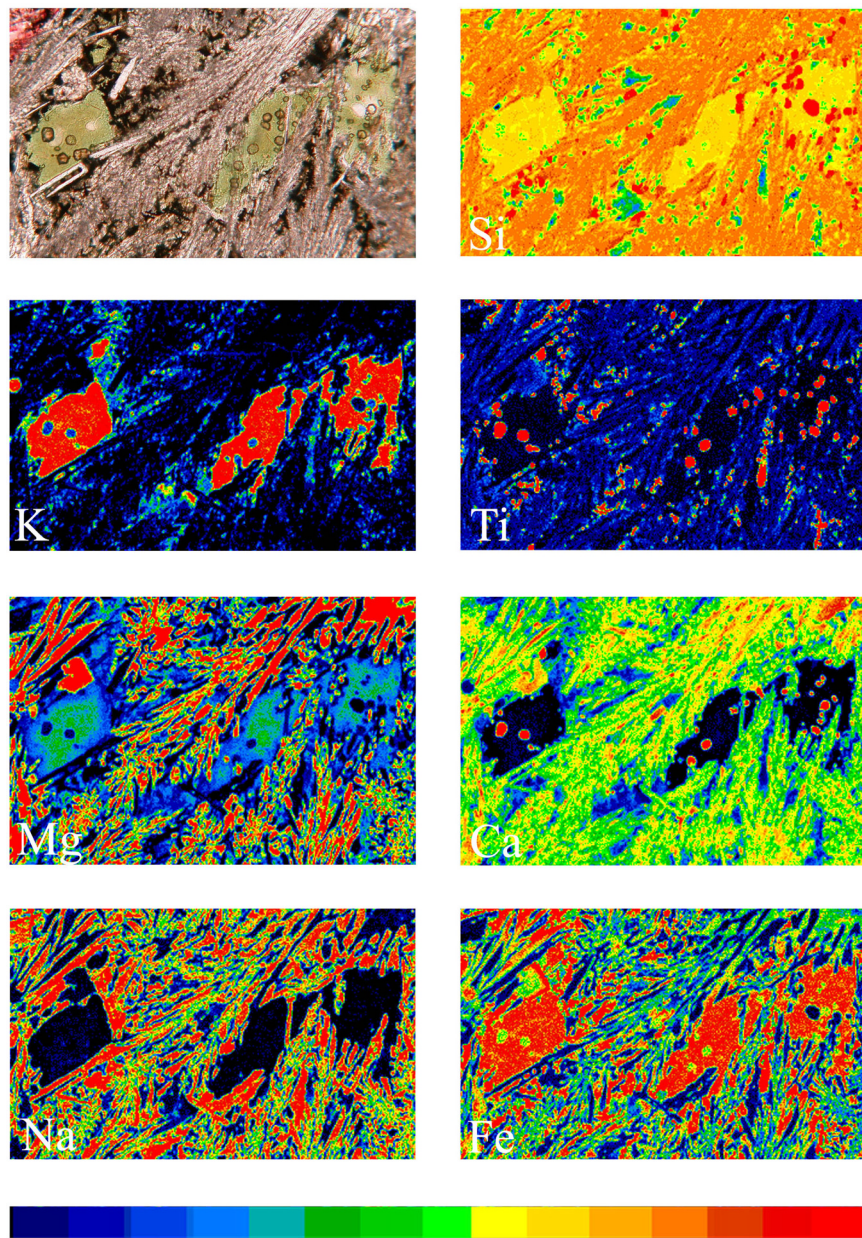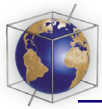
Figure 7. Photomicrograph (top left) in plane parallel light and maps of element (Si, Fe, Ti, Ca, Na, Mg, and K) distributions in the dark green alteration halo of Sample 206-1256D-65R-1, 105–109 cm (see also Figure 3a). Three zones of celadonite (Si, Fe, and K rich) and hydroschorlomite (Ca, Ti, and Fe rich) are clearly distinguished; they replace olivine (left, center?) or fill miarolitic voids (center?, right). Hydroschorlomite crystals observed on the photomicrograph but lacking on the chemical maps (e.g., red on the Ti map) are beneath the surface of the thin section. The thin yellow rim of hydroschorlomite crystals on the Ti map is an artifact due to the lower thickness of mineral at its periphery penetrated by the electron beam. Silica mineral globules (red on the Si map) appear not to be restricted to the celadonitic areas. Note the abundance of very fine grained titanomagnetite (field of view: 650 μm). Color scale: the concentration ranges from black (hole) to dark blue (background) to red (maximum concentration in the scanned zone).
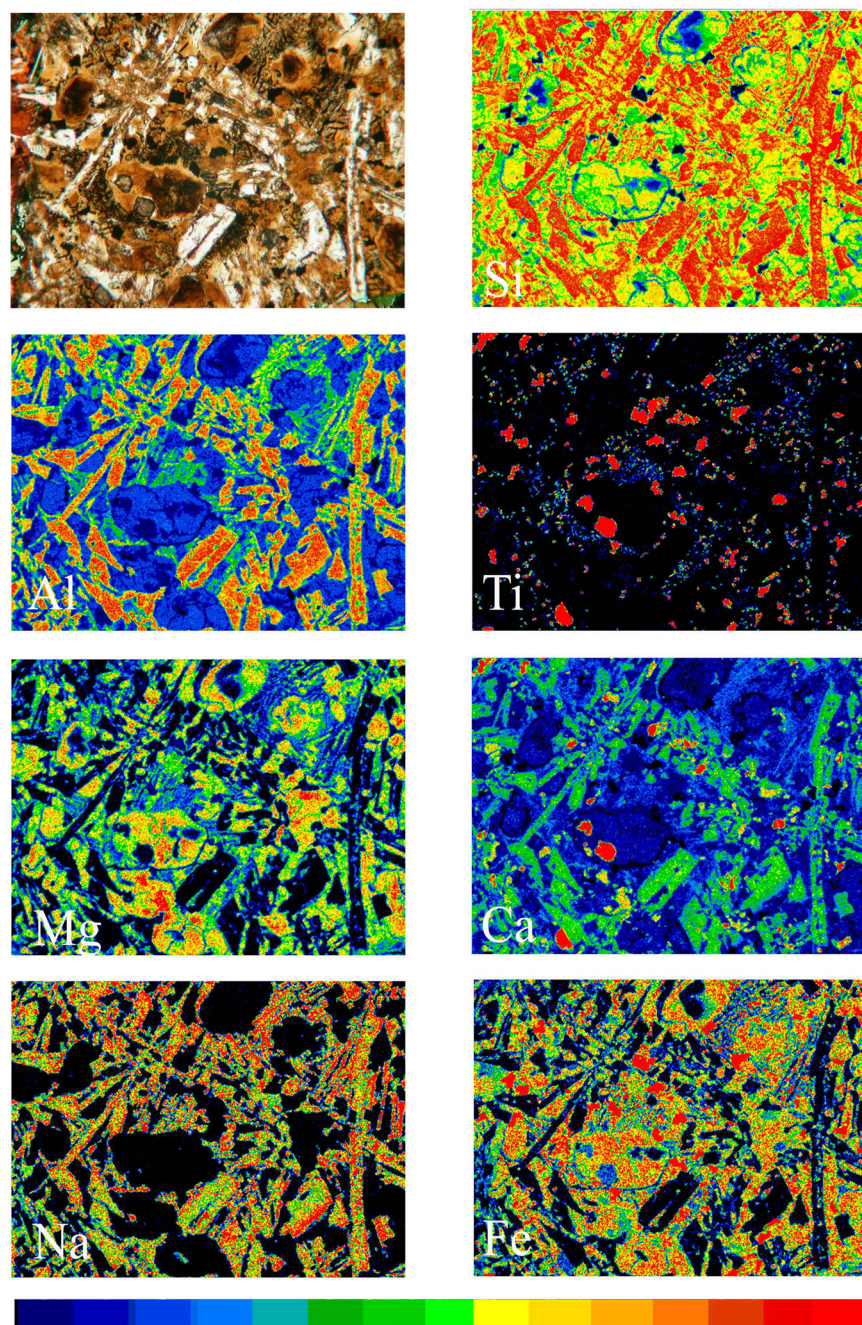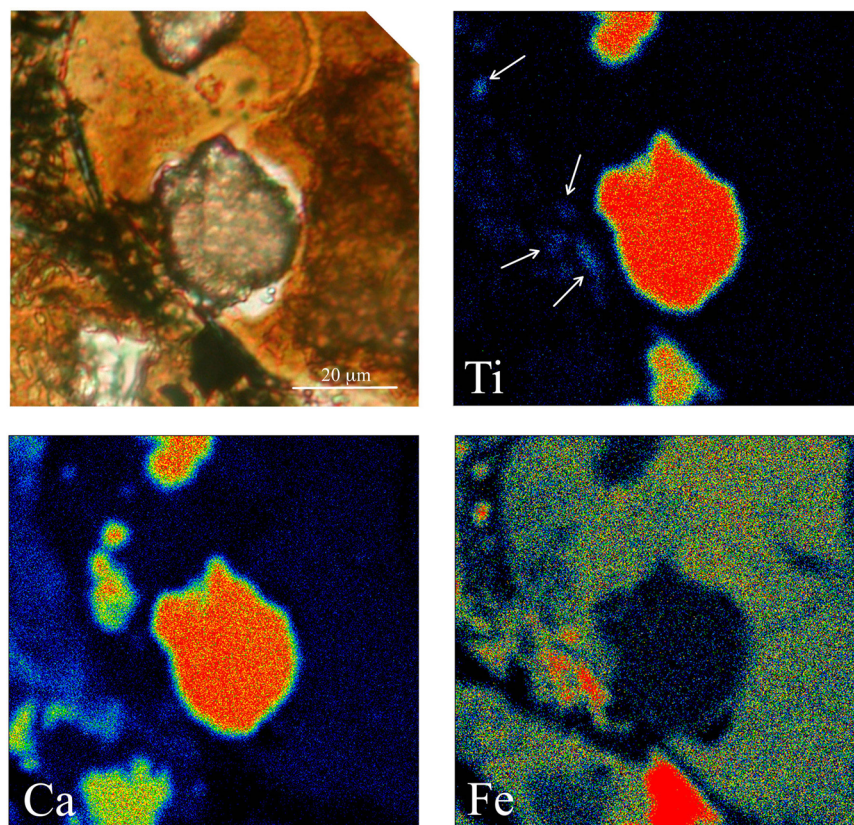
Figure 8. Photomicrograph (top left) in plane parallel light and maps of element (Si, Fe, Ti, Ca, Na, Mg, and Al) distribution in the orange alteration halo of Sample 206-1256D-74R-2, 81–85 cm (see also Figures 4c and 4d). Abundant orange brown saponite fills vesicles and replaces plagioclase and interstitial areas (field of view: 650 μm). Hydroschorlomite (red on both Ca and Ti maps) is associated with saponite in these three modes of occurrence.

Figure 9. Detail of Figure 7: photomicrograph in plane parallel light (top left) and maps of chemical elements (Ti, Ca, Fe) distributions in the orange alteration halo of Sample 206-1256D-74R-2, 81–85 cm. Two hydroschorlomite crystals (red on Ti map) occur in a saponite vesicle. Note the large (10 μm) Fe- and Ti-rich oxide crystal at the bottom of the picture and small elongated (width: 1 μm) Fe-rich, Ti-poor oxide crystals (arrows).

[18] Hydroschorlomite associated with saponite has SiO_2, CaO and K_2O contents similar to those of the celadonite-associated EMP end-members (CCOR), but has slightly lower FeO_t contents (Table A1, Figure 5). MgO contents of hydroschorlomite associated with saponite (0.5–0.8 wt%) are higher than in the CCOR and may be due to the presence of saponite inclusions (associated saponite has MgO ranging from 9.0 to 13.5 wt%; Table A2). Using the same method as above, but assuming that hydroschorlomite has MgO = 0 wt% yields the composition of the saponite-associated EMP end-member, labeled SCOR (Table 2, Figure 5).

4.3. Chemical Mapping

[19] In order to supplement the observations presented above and to examine the sites of crystallization of hydroschorlomite, we carried out chemical mapping on both the dark green alteration halo of Sample 206-1256D-65R-1, 105–109 cm (Figure 7) and the orange halo of Sample 206-

1256D-74R-2, 81–85 cm (Figures 8 and 9). Figure 7 confirms that (1) hydroschorlomite is not zoned; (2) hydroschorlomite is always associated with celadonite in this sample, whereas silica mineral globules are not restricted to the celadonitic areas; (3) a very fine grained (<10 μm) population of titanomagnetite occurs; and (4) clinopyroxene and plagioclase constitute the plumose texture. Figure 8 shows that (1) hydroschorlomite is associated with orange brown phyllosilicate occurring as a vesicle filling and replacement of interstitial areas and rarely replacing plagioclase and (2) hydroschorlomite is not zoned. Figure 9 shows that the largest (>10 μm) massive opaque crystals are Ti and Fe-rich whereas small (width = 1 μm, length < 10 μm) skeletal opaque crystals are Fe-rich and Ti-poor.

4.4. SEM

[20] The hydroschorlomite-bearing vesicles were investigated by SEM, both on a broken surface of basalt (Sample 206-1256D, 67R-1, 47–50 cm;
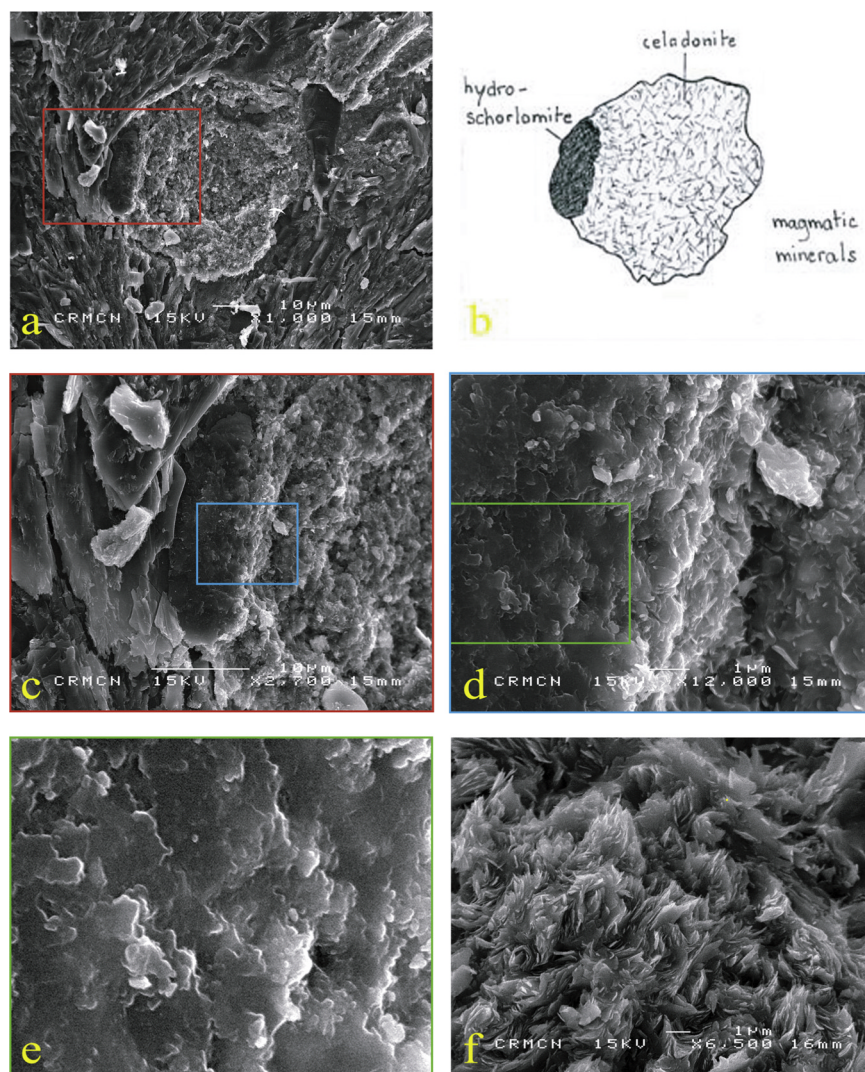
Figure 10. Back scattered electron images obtained by SEM on the rough surface of a piece of Sample 206-1256D-67R-1, 47–50 cm. (a) General view of a celadonite and hydroschorlomite vesicle in the dark green alteration halo adjacent to vein (Figure 10f). (b) Schematic drawing of Figure 10a. (c–e) Successive "enlargements" of Figure 10a. (f) Celadonite in vein.

Figure 10) and in thin section (Sample 206-1256D, 67R-3, 5–8 cm; Figures 11, 12, and 13) in order to further document hydroschorlomite morphology and mineral relationships. Hydroschorlomite crystals have irregular boundaries (Figures 10a, 10b, and 10c) and display an oriented, platy texture similar to cleavage on the fractured surface (Figures 10d and 10e), in contrast to the platy but randomly oriented texture of the adjacent clay mineral (Figure 10f). In polished thin sections, hydroschorlomite commonly appears to have diffuse boundaries (Figures 10e, 11d, and 12d). This is also apparent when the hydroschorlomite surface is imaged within concavities (Figure 11f). Hydro-

schorlomite may enclose tiny skeletal titanomagnetites (Figures 10c and 11c), and the size, shape and distribution of hydroschorlomite are similar to those of chalcedony (Figures 13c and 13d). SEM/EDS analyses of hydroschorlomite (Table A7) confirm the presence of this mineral. We consider these SEM/EDS analyses to be semi-quantitative, however, and they are not used in the following discussions.

4.5. Micro-Raman Spectroscopy

[21] Micro-Raman Spectroscopy (MRS) confirms the presence of structural OH in a small (30 μm in diameter) hydrogarnet crystal that is associated
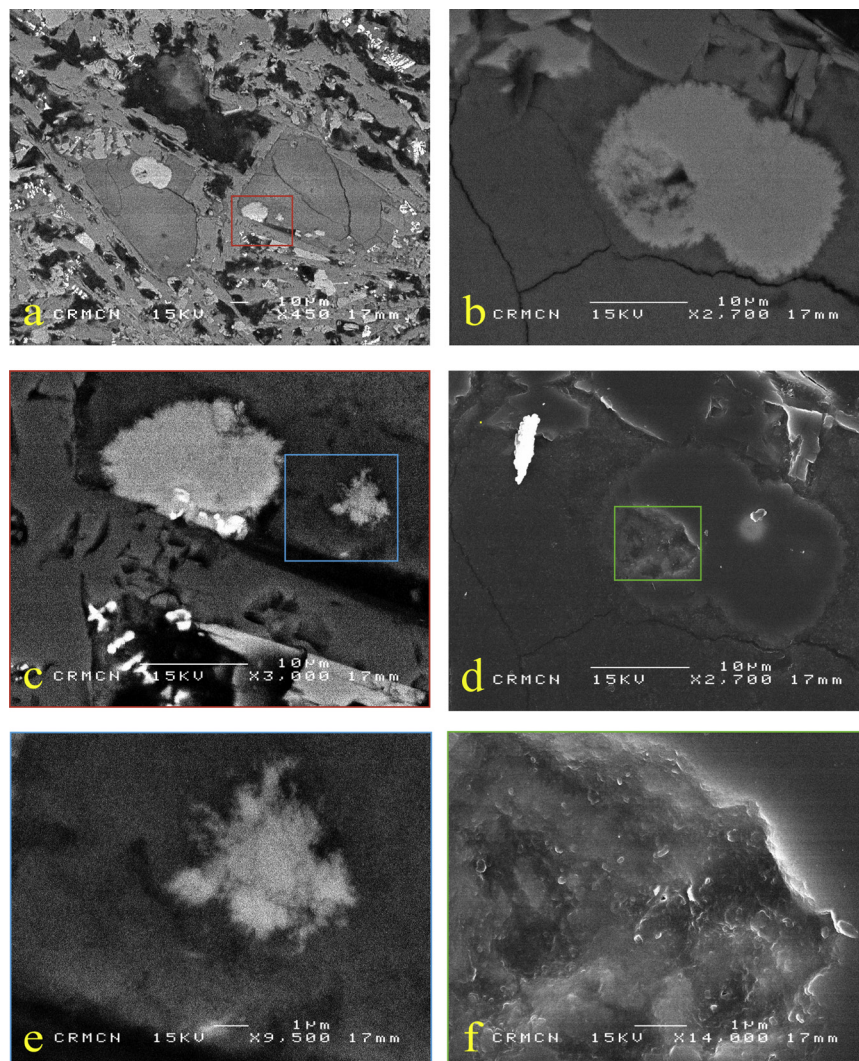
Figure 11. SEM image of two (probable) olivine microcrystals completely replaced by celadonite (medium gray) and hydroschorlomite (very light gray) in thin section from Sample 206-1256D-67R-3, 5–8 cm (Figures 11a, 11b, 11c, and 11e are secondary electrons images; Figures 11d and 11f are back scattered electron images). (a) General view. Note the fine-grained skeletal titanomagnetite (white). (b and d) Detail of two coalescing hydroschorlomite globules in Figure 11a. (c) Other detail of Figure 11a. (e) Detail of Figure 11c. Note the very diffuse appearance of hydroschorlomite. (f) Detail of a cavity in hydroschorlomite (Figure 11d).

with celadonite in a vesicle from Sample 206-1256D-70R-2, 8–12 cm. We obtain an OH vibration for garnet at 3545 cm^{-1} (Figure 14a). This is very close to the value of 3564 cm^{-1} for schorlomite using infrared spectroscopy [*Locock et al.*, 1995; *Amthauer and Rossman*, 1998] and confirms the presence of OH groups in the garnet from Hole 1256D. The schorlomite reported by *Locock et al.* [1995] contains 0.036 wt% H$_2$O$^+$. The MRS spectrum of hydroschorlomite (in blue in Figure 14b) is a superposition of garnet and celadonite spectra in the zone 2800–3200 cm^{-1}, consistent with the EMP analyses discussed previously representing

mixtures of these two minerals. This is also suggested by the diffuse boundaries of hydroschorlomite crystals when observed by SEM in back scattered electrons (Figures 11e, 12d, and 13d).

4.6. TEM

[22] In order to examine the nature of the intergrowth of celadonite and hydroschorlomite, it was necessary to carry out TEM studies on a section clearly located in the central part of a hydroschorlomite globule. A small section ~80 nm thick was milled from a hydroschorlomite globule from Sam-
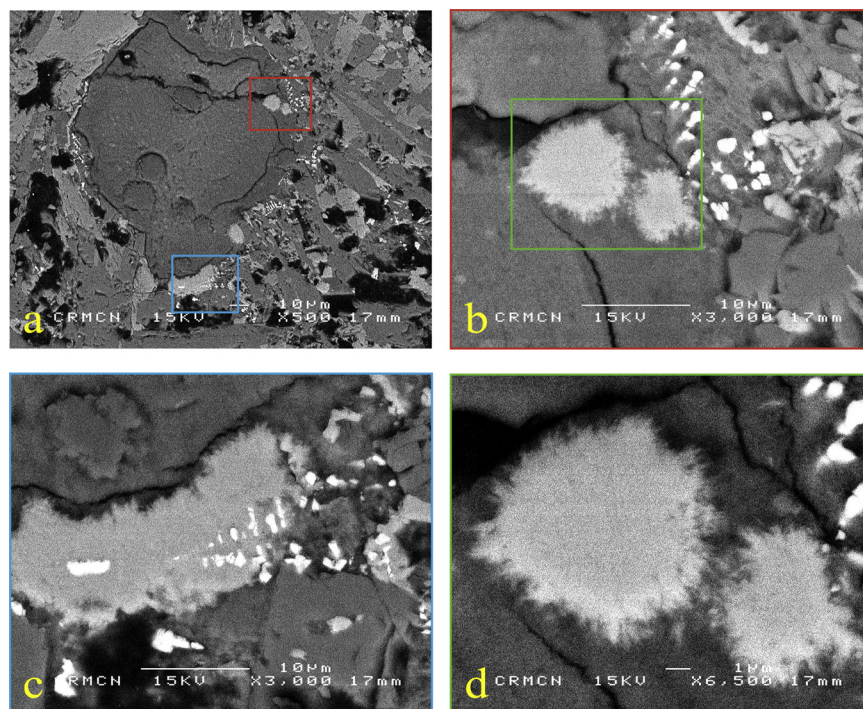
Figure 12. SEM image of vesicle filled with celadonite (medium gray), hydroschorlomite (very light gray), and silica mineral globules (medium gray, bordered by dark gray) in thin section from Sample 206-1256D-67R-3, 5–8 cm (Figures 12a, 12b, 12c, and 12d are back scattered electron images). (a) General view. Note the fine-grained skeletal titanomagnetite (white). (b and d) Detail of two hydroschorlomite globules of Figure 12a. Note their very diffuse boundaries. (c) Other detail of Figure 12a. Note the silica mineral globule (medium gray; top left) and the skeletal titanomagnetite partly included in hydroschorlomite.

ple 206-1256D-70R-2, 8–12 cm (Figure 15a). TEM observations at relatively low magnification reveal a chaotic surface of unoriented crystallites (Figure 15b). At higher magnification, numerous crystallites of phyllosilicate are more clearly observed, some of them on the surface and others within the section. The phyllosilicate crystallites show no preferential orientation and optically appear more abundant than hydroschorlomite, recognized by its lack of visible layers (Figures 15c and 15d). However, chemical analyses do not support this observation since many analyses of the phyllosilicate crystallites have compositions closer to hydroschorlomite than to celadonite. This misleading visual impression can be explained by the fact that the section is thicker than the celadonite crystallites, which diffract more strongly than the hydrogarnet.

[23] Thirty-four chemical analyses were made using TEM, both on apparently celadonite-poor and celadonite-rich parts of the TEM section (Table A8). Na was measured on only 4 of the 34 analyses in order to avoid interferences with gallium, which was used for ion milling and contam-

inates the surface of the sample. In Figure 16, all oxides of the 30 Na-free analyses are plotted versus K_2O. Linear regressions allow determination of the contents of each oxide in the anhydrous hydroschorlomite end-member, where $K_2O = 0\%$ (labeled "TEM" in Table 2 and Figure 5). Linear regressions using the 4 analyses including Na_2O provide another end-member hydrochlorlomite composition (labeled "TEM Na" in Table 2 and Figure 5). Several elements (Mg, Mn, Cr, Zr, Y, Cl, P) present in small amounts are not taken into account in the end-member composition. When recalculated assuming 5% H_2O, the end-member compositions of hydroschorlomite determined by TEM are similar to those determined by EMP, although CaO is higher in the TEM end-member (30.9 wt%) (Figure 5).

5. Discussion

5.1. Composition of Hydroschorlomite

[24] The end-member hydroschorlomite from Hole 1256D has TiO_2 ranging from 26 to 29 wt%. Previously, the most titanium-rich garnet reported
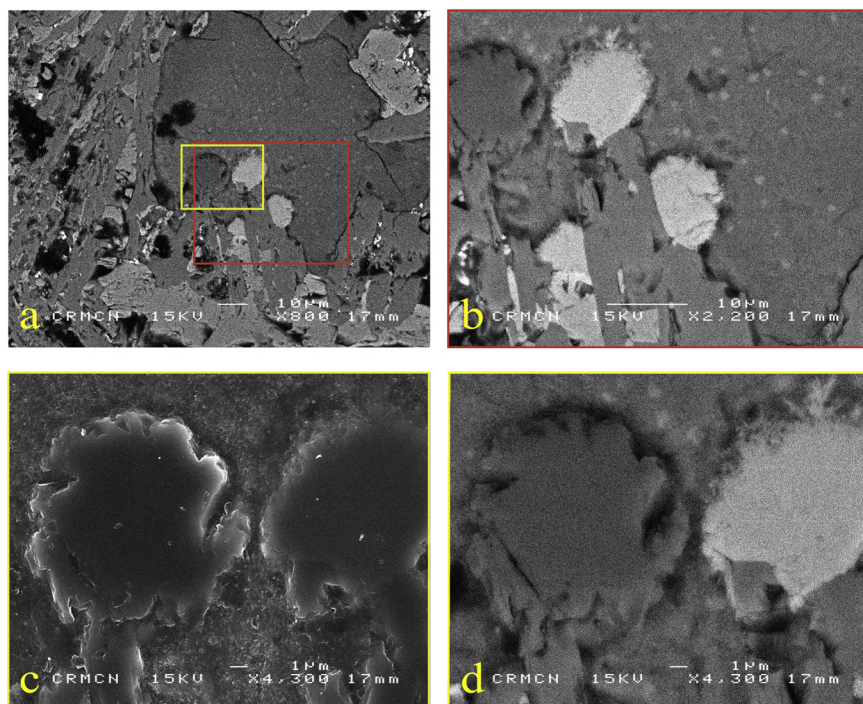
Figure 13. SEM image of vesicle filled with (or olivine replaced by?) celadonite (medium gray), hydroschorlomite (very light gray), and a silica mineral globule (medium gray, lined by dark gray) in thin section from Sample 206-1256D-67R-3, 5–8 cm (Figures 13a, 13b, and 13d are back scattered electron images; Figure 13c is a secondary electron image. (a) General view. (b) Detail of two hydroschorlomite globules of Figure 13a. (c and d) Other detail of Figure 13a: silica mineral (left) and hydroschorlomite (right) globules.

is schorlomite which occurs as an alteration product of ilmenite in syenite from Morotu, Sakhalin, and that contains up to 27.4 wt% TiO_2 [*Grapes et al.*, 1979]. The crystal chemistry of titanium-rich garnets, usually known as Ti-andradites, melanites or schorlomites, is quite complex and differs from that of other garnets, which may be described by the formula $(M^{2+})_3$ $(M^{3+})_2$ Si_3O_{12}. Almost all chemical analyses of Ti-free garnets indicate a 3:2:3 ratio for $M^{2+}:M^{3+}:Si^{4+}$. In contrast, chemical analyses of Ti-rich garnets indicate that they deviate from the above general formula in one or more of the following ways: the number of divalent cations (site X) exceeds 3.0; the number of trivalent cations (site Y) is less than 2.0; the number of quadrivalent cations (Z; Si+Ti) exceeds 3.0.

[25] The exact site-occupancy of Ti in the andradite-melanite-schorlomite series has long been the subject of discussion [e.g., *Zedlitz*, 1933; *Kunitz*, 1936; *Manning and Harris*, 1970; *Dowty*, 1971; *Huggins et al.*, 1977a, 1977b; *Amthauer et al.*, 1977; *Schwartz et al.*, 1980; *Merli et al.*, 1995]. Ti has been suggested to be present as Ti^{3+} or Ti^{4+} [*Zedlitz*, 1933; *Kunitz*, 1936; *Huggins et al.*, 1977a,
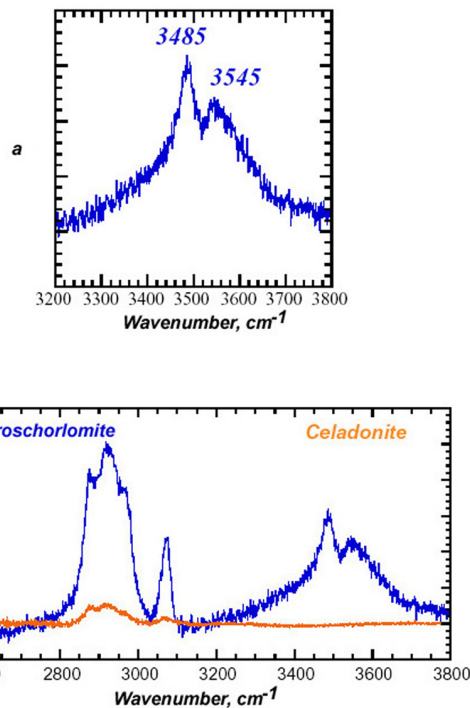
Figure 14. Micro-Raman spectra of minerals in a vesicle from Sample 206-1256D-70R-2, 8–10 cm: (a) hydroschorlomite and (b) hydroschorlomite (blue) and celadonite in the same vesicle but out of hydroschorlomite (orange).
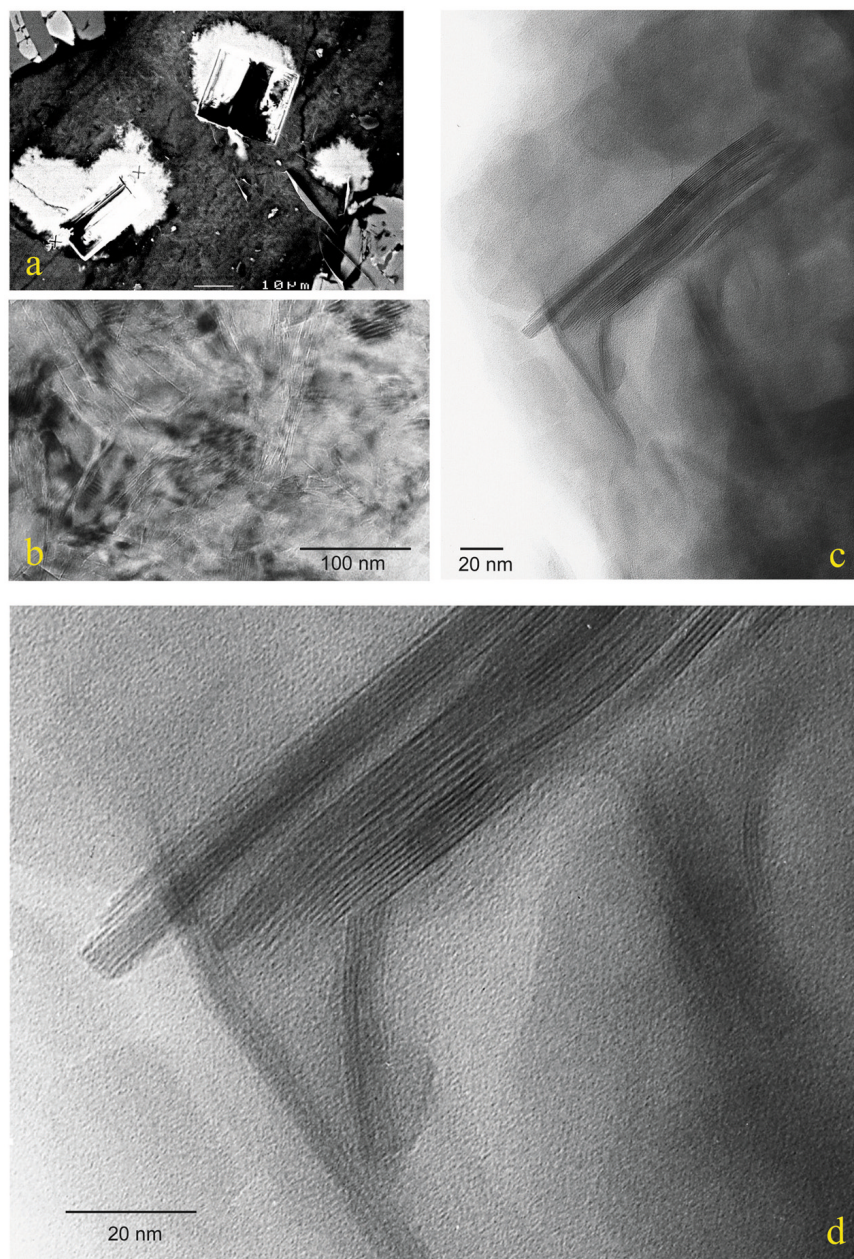
Figure 15. Investigation of a FIB slide of hydroschorlomite from Sample 206-1256D-70R-2, 8–12 cm. (a) General SEM view of celadonite (dark gray) and three hydroschorlomite (white) globules. The places where FIB cross-sectioning was made appear in black. The section at upper right failed. The lower left section, located between the crosses, was studied and is illustrated in Figures 15b, 15c, and 15d. (b) General TEM view of the surface of the FIB slide. Note the "chaotic" appearance. (c) Detail of Figure 15b. Areas rich in celadonite layers are clearly observed. See text for explanation. (d) Detail of Figure 15c. Note the 10 Å spacing of the celadonite layers.
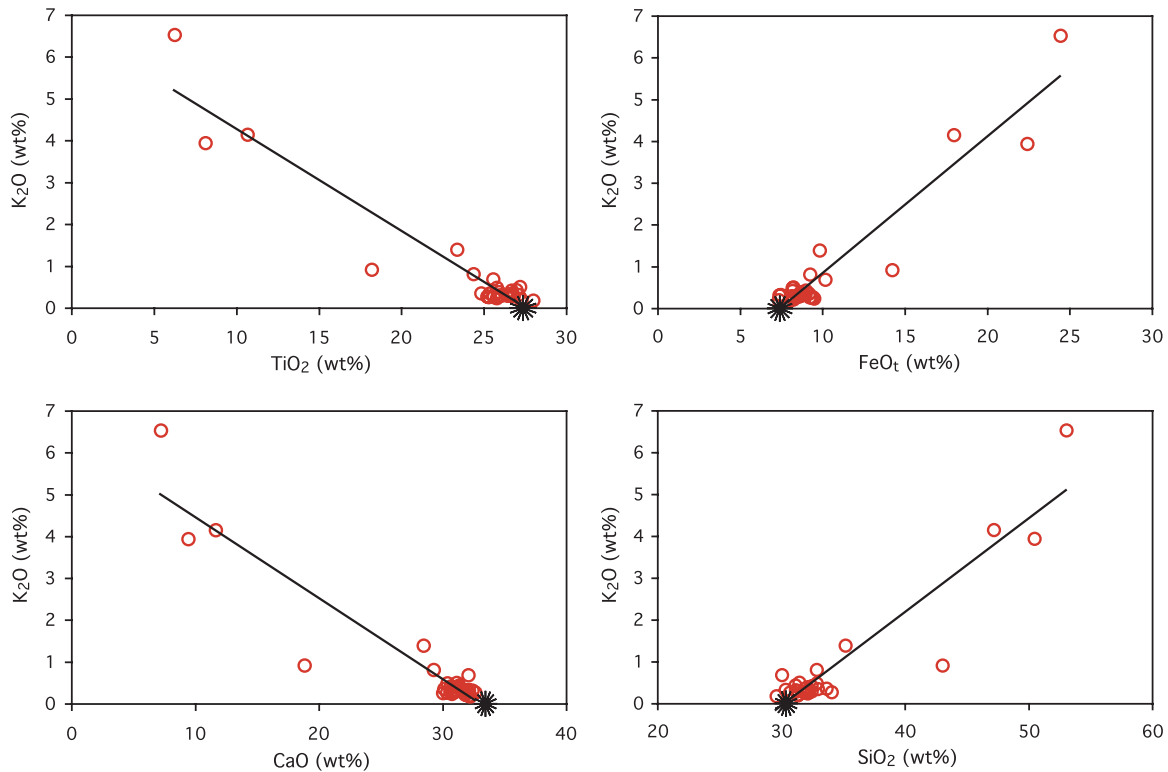
Figure 16. Composition of pure end-members of hydroschorlomite (black stars) from Sample 206-1256D-70R-2, 8–12 cm obtained by 30 TEM analyses (without determination of Na_2O) calculated on a water-free basis (open red circles). The correlations of K_2O with CaO, SiO_2, FeO_t, and TiO_2 contents confirm and illustrate the presence of celadonite inclusions in hydroschorlomite (see text for explanations).

1977b]. Studies by optical absorption spectroscopy [e.g., *Manning and Harris*, 1970; *Dowty*, 1971] have been carried out but could not provide accurate values for Fe^{2+}/Fe^{3+} or Ti^{3+}/Ti^{4+}. Mössbauer studies suggest that significant Ti^{3+} is generally present in Ti-rich garnets [*Burns and Burns*, 1971; *Burns*, 1972; *Whipple*, 1973; *Onuki et al.*, 1982], although the Ti^{3+} content of one schorlomite is negligible. From their investigation of eleven natural melanites and schorlomites by Mössbauer spectroscopy, *Huggins et al.* [1977b] show that Ti^{3+}/Ti_{total} exceeds 0.10 in only one sample, for which this ratio is as high as 0.25. These authors conclude that no one coupled-substitution mechanism can account for all the Ti in the garnet structure, and two or more of the following substitutions have to be invoked to account for the Ti substituted into garnet:

$$Ti^{4+} \Leftrightarrow Si^{4+}$$

$$M^{2+} + Ti^{4+} \Leftrightarrow 2M^{3+}$$

$$Ti^{3+} \Leftrightarrow M^{3+}$$
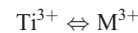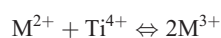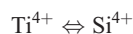
The same substitutions are proposed for synthetic garnets, where Ti^{4+} is mainly in octahedral sites with Fe^{3+} in tetrahedral sites [*Virgo and Huckenholz*, 1974]. In synthetic Ti-rich garnets, the relative preference for the tetrahedral site is in the order $Al \geq Fe > Ti$ [*Huggins et al.*, 1977a].

[26] The ideal formula of hydroschorlomite is X_3Y_2 $(Si_3O_{12})_{1-x}$ $(OH)_{4x}$ where X = Ca, Na, Mg, Fe^{2+}, Mn; Y = Al, Ti^{3+}, Ti^{4+}, Fe^{3+}, Cr, Zr; and x represents the number of H_4O_4 replacing SiO_4. Studies reporting occurrences of Ti-bearing hydrogarnets are rare. *Basso et al.* [1981] states that in natural Ti-bearing hydrogarnets, Ti is mainly as Ti^{3+} in the Y site.

[27] The oxidation states of iron and titanium in hydroschorlomite from Hole 1256D could not be determined, because the crystals are too small to be studied by Mössbauer or EELS. Moreover, the quantity of OH is uncertain. Consequently, we tested several ways of calculating structural formu-
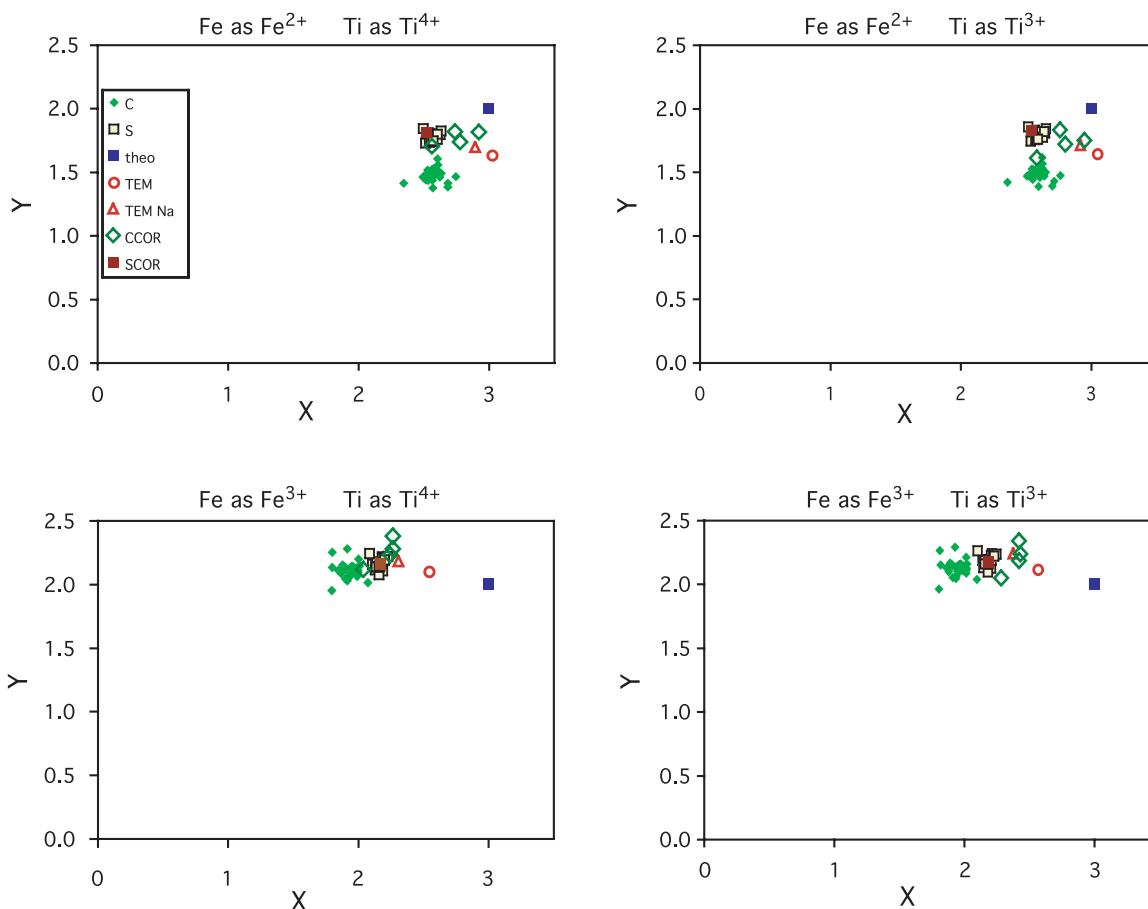
Figure 17. Occupation of sites X ($X = Ca + Na + Fe^{2+} + Mg + Mn + Y$) and Y ($Y = Ti^{4+} + Ti^{3+} + Al + Fe^{3+}Cr + Zr$) for Hole 1256D hydroschorlomite. Same legend as Figure 5. Various oxidation states are considered.

las: all the measured and calculated compositions of hydroschorlomite discussed above have been calculated considering all Fe as FeO and as Fe_2O_3, and all Ti as Ti^{4+} and as Ti^{3+}. A water content of 5% was assumed for the TEM end-members, consistent with totals of ∼95% for EMP analyses suggesting 5% H_2O. We obtain the best fit to the ideal formula when all iron is divalent for hydroschorlomite from Hole 1256D (Figure 17), whereas the oxidation state of titanium has only a minor effect on the filling of the crystallographic sites. Both celadonite- and saponite-associated EMP end-members plot very close to the theoretical values of X and Y, i.e., 3 and 2, respectively. Note that many published analyses of schorlomite [e.g., *Lehijärvi*, 1960] or hydroschorlomite [*Galuskin*, 2005] also have low calculated site occupancies (Figure 18). Melanite and schorlomite commonly contain significant Zr and V (0.1 and 0.2 wt%, respectively [*Huggins et al.*, 1977b]), which could in part account for these site vacancies.

5.2. Occurrence of Schorlomite and Hydroschorlomite

[28] Two major features of the garnets from Hole 1256D that are important and warrant discussion are (1) the high Ti content and (2) the hydrous nature of the garnet. In contrast to other garnets, which are found predominantly in metamorphic environments, the melanite and schorlomite varieties of andradite occur mainly as primary phases in alkaline igneous rocks and related rock types [e.g., *Donaldson and Dawson*, 1978] (see review by *Deer et al.* [1982]). Schorlomite has also been reported in calcium rich environments related to skarn formation and assimilation of limestone by basalt [*Kusachi et al.*, 1975; *Baker and Black*, 1980]. *Grapes et al.* [1979] report schorlomite associated with chamosite and microcrystalline leucoxene alteration of ilmenite in a pegmatitic syenite, interpreted to be the result of reaction with a late gas phase. This is the most Ti-rich garnet so far reported, but is slightly poorer in Ti than the
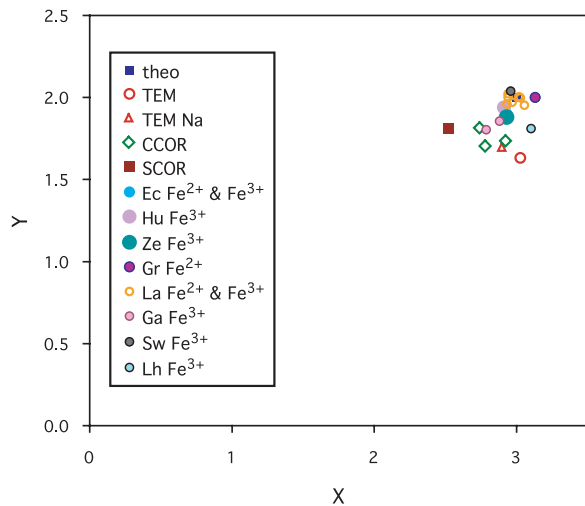
Figure 18. Occupation of sites X (X = Ca + Na + Fe^{2+} + Mg + Mn + Y) and Y (Y = Ti^{4+} + Ti^{3+} + Al + Fe^{3+} + Cr + Zr) for Ti-rich garnets and hydrogarnets. Analyses from Hole 1256D (same legend as Figure 5) are calculated considering all Fe as Fe^{2+} and all titanium as Ti^{4+}. The oxidation states of iron for analyses from other locations are given in the legend. Ec, *von Eckermann* [1974]; Hu, *Huggins et al.* [1977a]; Ze, *Zedlitz* [1933]; Gr, *Grapes et al.* [1979]; La, *Laverne* [1987]; Ga, *Galuskin* [2005]; Sw, *Switzer et al.* [1970]; Lh, *Lehijärvi* [1960]; theo, theoretical.

garnet from Hole 1256D (Figure 19). Only one occurrence of Ti-andradite is known in basalts from oceanic basement, where anhydrous melanite occurs in a vein of a single basalt sample from DSDP/ODP Hole 504B. The four observed crystals are zoned, with TiO_2 contents ranging from 0.7 to 6.4 wt% (Figure 19). They are interpreted as having precipitated from a mixture of deuteric and Ca-rich hydrothermal fluids at temperatures of 300–400°C [*Laverne*, 1983, 1987]. In contrast, Hole 1256D garnet is hydrated, is very TiO_2-rich (up to 29 wt%), is ubiquitous in the 90 deepest meters drilled during ODP Leg 206, and occurs as numerous crystals in alteration halos adjacent to veins.

[29] The single occurrence of hydrated schorlomite reported so far is that from the rodingite-like rocks of the Wiluy river, Yakutia. *Galuskina and Galuskin* [2003] mention schorlomite (TiO_2 13.5–14.5 wt%; Figure 19) with "considerable amounts of (OH) groups" (H_2O = 5 wt% [*Galuskin*, 2005]) and call it hydroschorlomite. Here hydrogrossular is an early metamorphic mineral with perovskite and titanite, and is partly replaced by hydroandradite and overgrown by hydroschorlomite. Rodingites typically form in Ca-metasomatic environments, and I. Galuskina (personal communication, 2005) suggests that low pH is necessary to solubilize Fe and Ti to
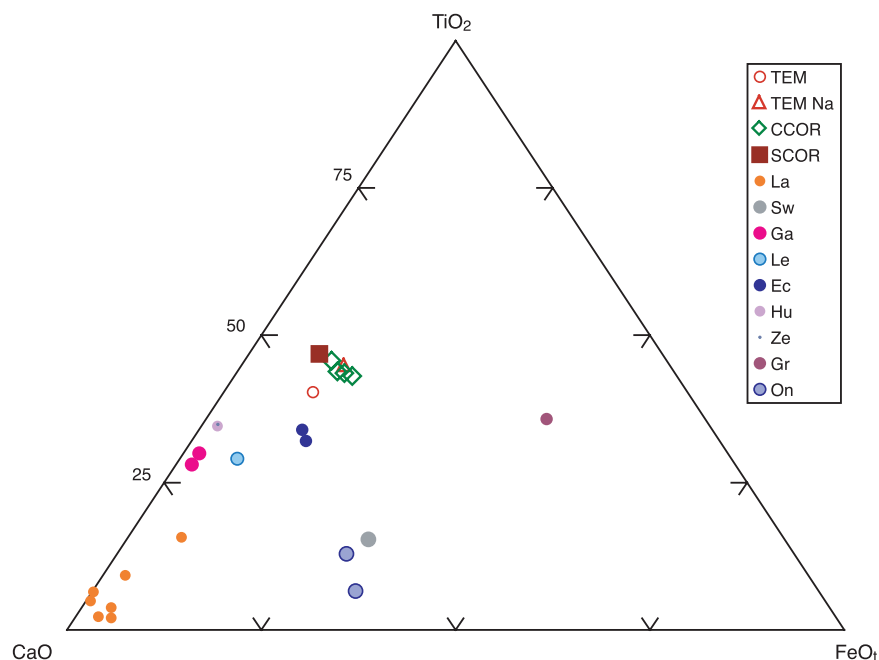
Figure 19. TiO_2-CaO-FeO_t ternary diagram comparing the hydroschorlomite compositions from Hole 1256D with Ti-rich andradite and schorlomite from various locations. Same symbols as Figure 18; On is data from *Onuki et al.* [1982].

form hydroschorlomite in these rocks. However, pH may be less important where Ti-garnet replaces a Ti-bearing phase, such as ilmenite or titanomagnetite. The composition of hydrothermal garnets depends on temperature and fluid composition (pH, oxygen fugacity, and salinity [*Jamtweit et al.*, 1995]). Hydroschorlomite chemically similar to that in Hole 1256D has been synthesized by the aging of precipitated gels at 85–105°C and 1 atm in NaOH solutions of pH 13.5 [*Ito and Frondel*, 1967]. In their IR spectroscopy study of twenty-two natural and two synthetic andradite samples, containing up to 6 wt% H_2O, *Amthauer and Rossman* [1998] show that those formed at low-temperature contain the most OH^-.

5.3. Formation of Hydroschorlomite in Hole 1256D

[30] Textural observations suggest that hydroschorlomite formed simultaneously with celadonite and the orange-brown saponitic phyllosilicate, and thus can be related to the same general alteration processes that formed these phases. Oxygen isotope analyses of celadonite, saponite, chalcedony, and quartz from Hole 1256D basalts suggest formation at temperatures up to ~100°C (J. Alt, unpublished data, 2005).

[31] Dark celadonite-bearing alteration halos occur in very young oceanic basalts and are enriched in iron and alkalis relative to the host basalts, leading to the interpretation that celadonite and the associated dark alteration halos form from upwelling distal hydrothermal fluids (e.g., summary by *Alt* [2004]). Such fluids are enriched in iron, alkalis, and calcium relative to seawater and are depleted in magnesium. In contrast, celadonite-free orange-brown halos are interpreted to result from interaction with seawater at high integrated water/rock ratios [e.g., see *Alt*, 2004]. Hydroschorlomite occurs both in dark celadonite-bearing halos and in celadonite-free orange-brown halos. Thus hydroschorlomite appears to form from more or less evolved seawater and hydrothermal fluids, over a wide range of oxidation potentials. A critical requirement for hydroschorlomite formation, however, is availability of Ti.

[32] Titanomagnetite breakdown is required to provide the titanium necessary to form hydroschorlomite. Several populations of different sizes of titanomagnetite occur in Hole 1256D basalts. Textural observations indicate that, in contrast to unaltered large (>10 μm) titanomagnetite, the very fined grained (1 × 10 μm) skeletal titanomagnetite could be replaced by a Ti-poor magnetite in the

surrounding rocks (Figure 9). Titanium released during this reaction could contribute to hydroschorlomite in vesicles and interstices. Still smaller titanomagnetite may be present as well, as suggested by <0.5 μm crystals shown in Figure 12. *Xu et al.* [1997a, 1977b] and *Zhou et al.* [1997, 2000, 2001] report different size populations of primary titanomagnetite in MORB. The smallest crystals, located in the glassy matrix, are globular and range from 0.5 to <0.05 μm in diameter. Titanomagnetite is observed as inclusions in hydroschorlomite and fine-grained Ti-poor magnetite is associated with hydroschorlomite in Hole 1256D, but pseudomorphs of titanomagnetite by hydroschorlomite have not been observed. However, if it is tiny interstitial titanomagnetite grains that are altered and provide the Ti for hydroschorlomite, then this could have a significant effect on magnetic properties, as it is these tiny (<1 μm) grains that exhibit single-domain superparamagnetic behavior and have the greatest influence on magnetic properties of MORB [*Zhou et al.*, 2000].

[33] The calcium necessary to form hydroschorlomite is released during the breakdown of plagioclase and its replacement by smectite and/or albite and to a lesser degree by the breakdown of glass, which is a minor constituent of the matrix. Iron may derive from the alteration of glass, olivine, and possibly titanomagnetite or could be from circulating fluids. The volcanic section of the oceanic crust is typically altered at low temperatures, less than about 100°C (see review by *Alt* [2004]). Alteration in Hole 1256D occurred at relatively high temperatures (up to ~100°C) but did not significantly differ from many other oceanic drilling sites. The first appearance of albite and smectite replacing plagioclase at 625 mbsf, and the extensive breakdown of plagioclase below 661 mbsf coincide with the appearance of small amounts of mixed-layer smectite-chlorite and generally increasing temperatures as indicated by oxygen isotope data for secondary minerals (J. Alt, unpublished data, 2005). The depth occurrence (661–749 mbsf) of hydroschorlomite coincides with this general increase in temperature and overall intensity of alteration with depth. However, titanite, which forms at greenschist facies conditions (i.e., at temperatures >250°C) and has a composition close to that of hydroschorlomite, is not present in this depth interval. We thus propose that hydroschorlomite forms during low-temperature alteration of titanomagnetite at conditions somewhat below the stability limit of titanite. The secondary mineralogy of basalts does not vary significantly over temper-

Table A1 (Representative Sample). Representative Electron Microprobe Analyses of Hydroschorlomite From Hole 1256D[a] [The full Table A1 is available in the HTML version of this article at http://www.g-cubed.org]

Analysis run	B7	B7	B7	B7	B7	B7	B8	B8	B8	B8	B8	B4	B4	B4	B4	B5
Analysis number	85	88	94	98	114	115	1	4	6	7	8	136	137	154	155	9
Hole	1256D	1256D	1256D	1256D	1256D	1256D	1256D	1256D	1256D	1256D	1256D	1256D	1256D	1256D	1256D	1256D
Core section	63R-1	63R-1	63R-1	63R-1	63R-1	63R-1	63R-1	63R-1	63R-1	63R-1	63R-1	65R-1	65R-1	65R-1	65R-1	65R-1
Interval, cm	50–53	50–53	50–53	50–53	50–53	50–53	50–53	50–53	50–53	50–53	50–53	105–109	105–109	105–109	105–109	105–109
Ass mal	cel	cel	cel	cel	cel	cel	cel	cel	cel	cel	cel	cel	cel	cel	cel	cel
SiO_2	34.22	35.14	34.27	35.13	35.21	35.18	33.72	33.82	34.50	34.29	32.41	33.20	33.35	35.09	34.10	34.45
TiO_2	23.73	22.88	23.77	22.83	22.75	22.02	23.95	22.65	21.35	23.76	21.57	22.97	24.95	24.13	23.53	23.27
Al_2O_3	1.80	1.87	1.74	2.06	2.11	2.44	1.91	1.85	2.03	1.94	1.83	1.62	1.62	1.72	1.76	1.64
CaO	23.75	22.57	23.87	22.66	22.72	21.45	23.41	22.36	21.52	23.25	21.28	22.60	24.20	22.99	23.45	23.68
Na_2O	0.09	0.12	0.09	0.15	0.08	0.20	0.10	0.17	0.15	0.15	0.13	0.07	0.07	0.12	0.07	0.06
K_2O	1.10	1.26	1.11	1.64	1.42	1.42	0.81	1.15	1.19	1.20	1.27	0.94	0.68	1.05	0.98	0.82
FeO	9.36	10.36	9.18	9.77	9.44	8.98	9.96	10.95	12.25	9.32	13.94	12.92	9.45	9.80	10.23	10.19
MgO	0.59	0.67	0.53	0.76	0.67	0.87	0.58	0.61	0.57	0.65	0.58	0.56	0.39	0.65	0.75	0.60
MnO	0.03	0.07	0.03	0.01	0.06	0.02	0.00	0.03	0.00	0.05	0.00	0.00	0.11	0.00	0.00	0.00
P_2O_5	0.00	0.03	0.00	0.04	0.00	0.00	0.00	0.01	0.05	0.04	0.00	0.02	0.00	0.02	0.00	0.00
Cl	0.04	0.07	0.01	0.07	0.00	0.02	0.03	0.08	0.08	0.05	0.09	nd	nd	nd	nd	0.00
F	0.61	0.47	0.56	0.00	0.00	0.00	0.00	0.95	0.41	0.69	0.00	nd	nd	nd	nd	0.00
Cr_2O_3	0.16	0.05	0.00	0.00	0.00	0.00	0.00	0.04	0.00	0.00	0.04	0.03	0.00	0.07	0.04	0.02
ZrO_2	0.00	0.06	0.00	0.16	0.03	0.00	0.05	0.00	0.00	0.13	0.00	nd	nd	nd	nd	nd
Y_2O_3	0.00	0.00	0.06	0.00	0.00	0.11	0.06	0.00	0.01	0.08	0.14	nd	nd	nd	nd	nd
Total	95.46	95.62	95.21	95.27	94.50	92.73	94.59	94.67	94.12	95.60	93.28	94.92	94.82	95.64	94.90	94.74

[a] Electron microprobe analyses are in weight percent. All iron expressed as FeO. ass mal, associated mineral; cel, celadonite; ob sap, orange-brown saponitic phyllosilicate; nd, not determined. Data include some analyses from *Laverne* [2006]. As discussed in the text, the majority of these analyses include both hydroschorlomite and microscopic inclusions of the associated phyllosilicate.

Table A2. Representative Electron Microprobe Analyses of Orange-Brown Saponitic Phyllosilicate From the Hydroschorlomite-Bearing Sample 206-1256D-74R-2, 81–85 cm[a]

Analysis run	B7	B7	B7	B7	B7	B7	B7	B7	B7
Analysis number	15	16	20	41	46	49	63	69	71
Hole	1256D	1256D	1256D	1256D	1256D	1256D	1256D	1256D	1256D
Core section	74R-2	74R-2	74R-2	74R-2	74R-2	74R-2	74R-2	74R-2	74R-2
Interval, cm	81–85	81–85	81–85	81–85	81–85	81–85	81–85	81–85	81–85
Occurrence	ves	ves	ves	inters	inters	inters	ves	pl cor	pl cor
SiO_2	40.27	40.86	40.66	39.20	40.00	38.78	38.14	38.82	39.73
TiO_2	0.12	0.04	0.17	0.04	0.06	0.00	0.22	0.00	0.05
Al_2O_3	8.63	8.95	9.24	8.95	8.78	8.73	7.95	9.28	10.25
CaO	3.60	3.44	3.92	3.71	4.69	3.73	3.44	2.84	3.15
Na_2O	0.23	0.19	0.17	0.23	0.20	0.46	0.20	0.41	1.43
K_2O	0.19	0.08	0.11	0.09	0.10	0.04	0.12	0.28	0.21
FeO_t	21.71	21.21	21.60	20.40	20.53	20.67	19.55	22.04	18.27
MgO	13.54	12.78	12.44	12.48	12.51	12.11	12.64	10.66	8.97
MnO	0.00	0.09	0.06	0.02	0.04	0.04	0.15	0.01	0.00
P_2O_5	0.00	0.04	0.01	0.00	0.00	0.00	0.00	0.01	0.00
Cl	0.00	0.06	0.02	0.32	0.07	0.48	0.08	0.10	0.17
F	0.00	0.00	0.02	0.00	0.00	0.26	0.36	0.00	0.08
Cr_2O_3	0.00	0.02	0.00	0.00	0.04	0.00	0.04	0.05	0.00
ZrO_2	0.00	0.14	0.09	0.00	0.02	0.00	0.00	0.00	0.00
Y_2O_3	0.00	0.00	0.00	0.00	0.11	0.00	0.00	0.04	0.00
Total	88.31	87.91	88.51	85.46	87.17	85.30	82.88	84.55	82.32

[a] Electron microprobe analyses are in weight percent. All iron expressed as FeO. ves, vesicle filling; inters, interstitial; pl cor, replacing core of plagioclase microphenocryst.

atures of near 0°C up to ~100–150°C, so the presence of hydroschorlomite may be a sensitive indicator of alteration at temperatures of ~100–200°C.
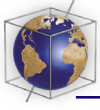
[34] Essentially all oceanic basalts are altered at low temperatures (<100°C) to variable extents. Most basement drill holes, however do not penetrate as deep into basement as Hole 1256D, and primary plagioclase is typically not altered as in Hole 1256D. The alteration temperatures in Hole 1256D at the depth of hydroschorlomite occurrence are at the high end of the range for altered oceanic basalts. It is likely these two factors, relatively high temperatures and breakdown of plagioclase, cause the formation of hydroschorlomite in Hole 1256D. The only other basement cores in oceanic crust that were altered under conditions similar to the lower volcanic section of Hole 1256D are from the lower volcanic section of DSDP/ODP Hole 504B [*Alt et al.*, 1985, 1996a, 1996b; *Honnorez et al.*, 1983]. However, a recent reexamination of these samples by one of us (CL) confirms the lack of hydroschorlomite in Hole 504B. A possible explanation for this is that insufficient Ca was available in Hole 504B. Another possibility is that the temperature gradient, from low-temperature alteration in the volcanic section to hydrothermal alteration in the dikes, was much steeper at Site 504 than at Site 1256.

This compressed thermal gradient from ~100°C to >250°C in Hole 504B may have prevented formation of hydroschorlomite at these transitional conditions. Further study of deeper cores from Hole 1256D drilled on Integrated Ocean Drilling Program Expedition 309 regarding the distribution of hydroschorlomite with respect to that of titanite and their relationships to low temperature and hydrothermal alteration processes may provide insight into this question.

6. Conclusions

[35] Hydroschorlomite is reported here for the first time in the oceanic crust. It occurs as small but almost ubiquitous crystals in the vein-related alteration halos at 661–749 mbsf in Hole 1256D. It is also the most titanium-rich garnet reported in the literature, with TiO_2 contents up to about 29 wt%. The MRS spectrum indicates the presence of OH groups, in accordance with the low total oxide percentages reflecting the presence of 3–5 wt% H_2O. Significant amounts of K_2O in EMP, SEM, and some of the TEM analyses of celadonite-associated hydroschorlomite indicate the presence of ~10–15% of celadonite as small crystallites (1–20 nm thick) within hydroschorlomite, as observed in TEM images.

Table A3   (Representative Sample). Representative Electron Microprobe Analyses of Celadonite and Celadonitic Phyllosilicates Associated With Hydroschorlomite From Hole 1256D, Leg 206[a] [The full Table A3 is available in the HTML version of this article at http://www.g-cubed.org]

Analysis run	B4	B4	B4	B4	B4	B4	B4	B4	B4	B4	B4	B5	B5	B5	B5	B5	B5
Analysis number	134	140	143	144	146	147	152	153	156	158	159	12	14	15	19	20	25
Hole	1256D	1256D	1256D	1256D	1256D	1256D	1256D	1256D	1256D	1256D	1256D	1256D	1256D	1256D	1256D	1256D	1256D
Core section	65R-1	65R-1	65R-1	65R-1	65R-1	65R-1	65R-1	65R-1	65R-1	65R-1	65R-1	65R-1	65R-1	65R-1	65R-1	65R-1	65R-1
Interval, cm	105–109	105–109	105–109	105–109	105–109	105–109	105–109	105–109	105–109	105–109	105–109	105–109	105–109	105–109	105–109	105–109	105–109
Occurrence	grm	grm	dk grm	dk grm	dk grm	dk grm	dk grm	dk grm	dk grm	yel grm	dk grm	yel grm	yel grm	yell grm	dk grm	dk grm	yel grm
Analysis run	inters	inters	vein	vein	ol? inter?	ol? inter?	ol? inter?	ol? inter?	inter?	pl	vein	inters	inters	inters	ol? inter?	ol? inter?	ol? inter?
SiO_2	46.31	47.69	52.89	54.75	53.72	53.21	54.73	55.98	52.68	52.25	53.39	49.54	46.52	46.26	54.90	48.08	47.41
TiO_2	0.12	0.14	0.00	0.04	0.04	0.09	0.00	0.04	0.14	0.13	0.09	0.23	0.08	0.09	0.06	0.07	0.13
Al_2O_3	4.86	5.09	2.56	2.83	2.40	2.44	2.97	2.69	3.48	4.31	3.94	4.93	4.79	4.78	2.69	2.46	5.19
CaO	0.90	1.02	0.43	0.40	0.56	0.56	0.33	0.40	0.41	0.63	0.47	1.74	0.98	0.91	0.34	0.28	0.80
Na_2O	0.10	0.23	0.18	0.11	0.06	0.07	0.06	0.06	0.18	0.28	0.08	0.41	0.29	0.24	0.06	0.02	0.27
K_2O	6.08	5.83	8.20	8.91	8.67	8.21	8.80	8.85	7.82	7.73	7.89	5.96	5.88	6.15	8.97	7.42	5.49
FeO	19.10	18.53	25.16	22.74	22.88	25.10	22.02	22.46	23.55	24.16	23.72	20.64	19.32	18.71	23.96	19.77	17.89
MgO	4.51	5.22	3.30	4.72	4.18	3.27	4.64	4.66	3.31	3.12	3.18	3.92	5.00	4.81	3.97	3.94	5.56
MnO	0.01	0.00	0.04	0.00	0.00	0.00	0.00	0.00	0.00	0.02	0.05	0.00	0.00	0.00	0.05	0.04	0.00
P_2O_5	0.00	0.00	0.00	0.01	0.00	0.00	0.01	0.04	0.00	0.00	0.00	0.00	0.00	0.01	0.00	0.01	0.00
Cl	nd	nd	nd	nd	nd	nd	nd	nd	nd	nd	nd	0.14	0.20	0.23	0.07	0.05	0.25
F	nd	nd	nd	nd	nd	nd	nd	nd	nd	nd	nd	0.00	0.29	0.00	0.00	0.00	0.00
Cr_2O_3	0.00	0.10	0.00	0.00	0.05	0.00	0.00	0.00	0.04	0.04	0.00	0.00	0.00	0.00	0.00	0.00	0.00
Total	82.00	83.86	92.76	94.52	92.57	92.97	93.56	95.20	91.62	92.68	92.81	87.51	83.36	82.19	95.07	82.14	83.00

[a] Electron microprobe analyses are in weight percent. All iron expressed as FeO. dk grm, dark green; yel grm, yellow green; ves, vesicle filling; inters, interstitial; pl cor, replacing core of plagioclase microphenocryst; ol, replacing olivine.

Table A4. Representative Electron Microprobe Analyses of Iron Oxyhydroxides in Hydroschorlomite- and Celadonite-Bearing Samples From Hole 1256D, Leg 206[a]

Analysis run	B5	B5	B5	B5	B5	B5	B5	B5	B5
Analysis number	16	17	18	46	47	48	33	34	35
Hole	1256D	1256D	1256D	1256D	1256D	1256D	1256D	1256D	1256D
Core section	65R-1	65R-1	65R-1	65R-1	65R-1	65R-1	67R-1	67R-1	67R-1
Interval, cm	105–109	105–109	105–109	105–109	105–109	105–109	47–54	47–54	47–54
Occurrence	vein	vein	vein	vein	vein	vein	vein rim	vein rim	vein rim
SiO_2	6.16	6.07	5.83	6.03	5.81	6.35	6.42	6.22	6.29
TiO_2	0.06	0.02	0.00	0.00	0.07	0.00	0.20	0.25	0.39
Al_2O_3	0.98	0.76	0.93	0.21	0.21	0.28	1.21	1.13	1.22
CaO	0.99	0.99	0.89	0.94	0.79	1.15	0.88	1.00	0.84
Na_2O	0.00	0.05	0.07	0.11	0.11	0.02	0.04	0.04	0.09
K_2O	0.01	0.02	0.03	0.00	0.05	0.00	0.30	0.07	0.18
Fe_2O_3	78.76	80.00	78.94	80.71	81.98	79.65	78.86	78.04	78.78
MgO	0.26	0.27	0.36	0.28	0.31	0.30	0.19	0.24	0.29
MnO	0.13	0.14	0.09	0.14	0.02	0.19	0.00	0.03	0.00
P_2O_5	0.31	0.22	0.12	0.11	0.15	0.17	0.24	0.23	0.12
Cl	0.01	0.06	0.04	0.00	0.05	0.02	0.11	0.11	0.09
F	0.05	0.13	0.00	0.00	0.09	0.00	0.00	0.26	0.00
Cr_2O_3	0.00	0.00	0.05	0.02	0.02	0.00	0.00	0.00	0.04
Total	87.73	88.72	87.36	88.55	89.66	88.13	88.47	87.61	88.32

[a] Electron microprobe analyses are in weight percent. All iron expressed as Fe_2O_3.

[36] The occurrence of hydroschorlomite in different types of alteration halos suggests that its formation is not controlled by the composition of fluids circulating through the fractures, but rather is related to the availability of titanium from breakdown of tiny titanomagnetite grains in the host rock. Calcium is provided by the replacement of plagioclase by albite or saponite, and iron by the alteration of glass, olivine, possibly titanomagnetite and/or from circulating fluids.

[37] Hydroschorlomite formation is related to the general increase in temperature suggested by the

Table A5. Representative Electron Microprobe Analyses of Magmatic Plagioclase and Albite Replacing Core of Plagioclase Phenocryst in Hydroschorlomite-Bearing Sample 206-1256D- 67R-1, 47–50 cm[a]

Analysis run	B4	B5
Analysis number	188	28
Hole	1256D	1256D
Core section	67R-1	67R-1
Interval, cm	47–50	47–54
Type	pl	ab
SiO_2	50.09	68.82
TiO_2	0.02	0.02
Al_2O_3	30.37	20.31
CaO	15.45	0.50
Na_2O	2.90	10.60
K_2O	0.00	0.05
FeO	0.56	0.37
MgO	0.30	0.02
MnO	0.01	0.00
P_2O_5	0.01	0.04
Cl	nd	0.01
F	nd	0.20
Cr_2O_3	0.00	0.00
Total	99.71	100.94
An	74.6	2.5
Ab	25.4	97.1
Or	0.0	0.3

[a] Electron microprobe analyses are in weight percent. All iron expressed as FeO. pl, plagioclase; ab, albite; nd, not determined; An, anorthite; Ab, albite; Or, orthose.

Table A6. Electron Microprobe Analysis of Ti, Fe-oxide in a Hydroschorlomite-Bearing Sample From Hole 1256D[a]

Analysis run	B7
Analysis number	47
Hole	1256D
Core section	74R-2
Interval, cm	81–85
SiO_2	0.35
TiO_2	14.81
Al_2O_3	2.65
CaO	0.28
Na_2O	0.01
K_2O	0.00
Fe_2O_3	79.06
MgO	0.86
MnO	1.11
P_2O_5	0.07
Cl	0.00
F	0.04
Cr_2O_3	0.00
ZrO_2	0.13
Y_2O_3	0.00
Total	99.39

[a] Electron microprobe analyses are in weight percent. All iron expressed as Fe_2O_3.

Table A7. Chemical Analyses (in Weight Percent) of Hydroschorlomite Associated With Celadonite From Sample 206-1256D-67R-3, 5–8 cm Obtained by SEM, Recalculated on an Anhydrous Basis[a]

Analysis number	4	7	8
Hole	1256D	1256D	1256D
Core section	67R-3	67R-3	67R-3
Interval, cm	**5–8**	**5–8**	**5–8**
SiO_2	25.67	25.45	23.96
TiO_2	30.94	31.42	32.93
Al_2O_3	1.13	3.44	1.44
CaO	26.41	26.82	26.37
Na_2O	0,00	0,00	0,00
K_2O	0.93	1.39	2.50
FeO	14.92	11.49	10.67
MgO	0.00	0.00	2.14
Total	100.00	100.00	100.00

[a] Chemical analyses are in weight percent. All iron expressed as FeO.

breakdown of magmatic plagioclase, the formation of albite and mixed-layered smectite/chlorite. Hydroschorlomite represents an intermediate stage of breakdown of titanomagnetite into titanite, thus being an indicator of the transition between low-temperature alteration and hydrothermal alteration under sub greenschist facies conditions. Alteration of tiny grains of magnetite to hydroschorlomite may have important effects on magnetic properties of basalts.

Appendix A: Chemical Analyses of Hydroschorlomite and Associated Secondary Minerals

[38] Analyses of hydroschorlomite (Table A1), saponitic phyllosilicates (Table A2), celadonitic phyllosilicates (Table A3), iron oxyhydroxides (Table A4), plagioclase (Table A5), and Fe-Ti oxides (Table A6) were performed by electron microprobe. Additional analyses of hydroschorlomite were performed by SEM-EDS (Table A7) and TEM (Table A8). See sections 3, 4.2, 4.4, and 4.6 for analytical details and analysis of data.

Acknowledgments

Table A8. (**Representative Sample**). Chemical Analyses of Hydroschorlomite From Sample 206-1256D-70R-2, 8–12 cm Obtained by TEM, Recalculated on an Anhydrous Basis[a] [The full Table A8 is available in the HTML version of this article at http://www.g-cubed.org]

	1	2	3	4	5	6	7	8	9	10	11	12	13	14	15	16	17	18
SiO_2	43.02	31.47	53.00	32.05	31.31	31.85	32.11	30.04	32.00	32.94	32.06	30.67	32.43	31.12	32.44	50.47	47.16	29.59
TiO_2	18.19	27.18	6.23	25.91	27.23	25.57	25.78	25.55	25.28	25.37	25.89	25.25	26.68	26.97	26.03	8.11	10.66	27.99
Al_2O_3	3.29	1.40	2.56	1.70	1.20	1.20	1.66	1.47	0.62	1.08	1.51	3.34	1.67	1.21	1.60	4.09	5.22	2.02
CaO	18.82	31.12	7.21	31.30	31.81	31.70	30.73	32.09	32.61	31.55	31.63	30.00	30.63	31.29	31.05	9.42	11.64	32.22
Na_2O	nd	nd	nd	nd	nd	nd	nd	nd	nd	nd	nd	nd	nd	nd	nd	nd	nd	nd
K_2O	0.92	0.51	6.53	0.39	0.22	0.27	0.24	0.69	0.27	0.36	0.31	0.26	0.42	0.44	0.30	3.95	4.15	0.18
FeO	14.23	8.22	24.42	8.65	8.23	9.41	9.48	10.17	9.21	8.70	8.60	9.33	8.18	8.97	8.59	22.41	17.97	7.98
MgO	1.55	0.10	0.00	0.00	0.00	0.00	0.00	0.00	0.00	0.00	0.00	1.13	0.00	0.00	0.00	1.56	3.19	0.00
Total	100.00	100.00	100.00	100.00	100.00	100.00	100.00	100.00	100.00	100.00	100.00	100.00	100.00	100.00	100.00	100.00	100.00	100.00

[a] Chemical analyses are in weight percent. All iron expressed as FeO.

References

Alt, J. C. (1999), Very low grade hydrothermal metamorphism of basic igneous rocks, in *Very Low Grade Metamorphism*, edited by M. Frey and D. Robinson, pp. 169–201, Blackwell Sci., Malden, Mass.

Alt, J. C. (2004), Alteration of the upper oceanic crust: Mineralogy, chemistry, and processes, in *Hydrogeology of the Oceanic Lithosphere*, edited by H. Elderfield and E. Davis, pp. 456–488, Cambridge Univ. Press, New York.

Alt, J. C., and C. Laverne (2006), Data report: Chemical compositions of secondary minerals from Site 1256 basement, ODP Leg 206 [online], *Proc. Ocean Drill. Program, Sci. Results*, *206*. (Available at http://www-odp.tamu.edu/publications/206_SR/003/003.htm.)

Alt, J. C., C. Laverne, and K. Muehlenbachs (1985), Alteration of the upper oceanic crust mineralogy and processes in Deep Sea Drilling Project Hole 504B, Leg 83, edited by R. N. Anderson et al., *Initial Rep. Deep Sea Drill. Proj.*, *83*, 217–248.

Alt, J. C., et al. (1996a), Hydrothermal alteration of a section of upper oceanic crust in the Eastern Equatorial Pacific: A synthesis of results from DSDP/ODP Legs 69, 70, 111, 137, 140, and 148 at Site 504, in edited by J. C. Alt et al., *Proc. Ocean Drill. Program, Sci. Results*, *148*, 417–434.

Alt, J. C., D. A. H. Teagle, C. Laverne, D. Vanko, W. Bach, J. Honnorez, K. Becker, and P. A. Pezard (1996b), Ridge flank alteration of upper ocean crust in the eastern Pacific: A synthesis of results for volcanic rocks of Holes 504B and 896A, *Proc. Ocean Drill. Program, Sci. Results*, *148*, 435–450.

Amthauer, G., and G. R. Rossman (1998), The hydrous component in andradite garnet, *Am. Miner.*, *83*, 835–840.

Amthauer, G., H. Annersten, and S. S. Hafner (1977), The Mössbauer spectrum of ^{57}Fe in titanium-bearing andradites, *Phys. Chem. Miner.*, *1*, 399–413.

Baker, C. K., and P. M. Black (1980), Assimilation and metamorphism at a basalt-limestone contact, Tokatoka, New Zealand, *Min. Mag.*, *43*, 797–807.

Basso, R., A. Della Giusta, and L. Zefiro (1981), A crystal chemistry of a Ti-containing hydrogarnet, *Neues Jahr. Mineral Abh.*, *5*, 230–236.

Burns, R. G. (1972), Mixed valencies and site occupancies of iron in silicate minerals from Mössbauer spectroscopy, *Can. J. Spectrosc.*, *3*, 519–520.

Burns, R. G., and V. M. Burns (1971), Study of the crystal chemistry of titaniferous garnets by Mössbauer spectroscopy, *Geol. Soc. Am. Abstr. Programs*, *3*, 51–59.

Busigny, V., C. Laverne, and M. Bonifacie (2005), Nitrogen content and isotopic composition of oceanic crust at superfast spreading ridge: A profile in altered basalts from ODP Site 1256, Leg 206, *Geochem. Geophys. Geosyst.*, *6*, Q12O01, doi:10.1029/2005GC001020.

Cliff, G., and G. W. Lorimer (1975), The quantitative analysis of thin specimens, *J. Microsc.*, *103*, 203–207.

Deer, W. A., , R. A. Howie, and J. Zussman (Eds.) (1982), *Rock-Forming Minerals*, vol. 1A, *Orthosilicates*, 919 pp., Longman, New York.

Donaldson, C. H., and J. B. Dawson (1978), Skeletal crystallization and residual glass compositions in a cellular alkalic pyroxenite nodule from Oldoinyo Lengai. Implications for evolution of the alkalic carbonatite lavas, *Contrib. Mineral. Petrol.*, *67*, 139–149.

Dowty, E. (1971), Crystal chemistry of titanium and zirconian garnets; 1, Review and spectral studies, *Am. Mineral.*, *56*, 1983–2009.

Galuskin, E. (2005), Minerals of the vesuvianite rocks from the achtarandite rocks (Wiluy River, Yakutia) (in Polish), 191 pp., Univ. of Silesia Publish House, Katowice, Poland.

Galuskina, I., and E. Galuskin (2003), Garnets of the hydrogrossular – "hydroandradite" – "hydroschorlomite" series, *Spec. Pap. Mineral. Soc. Poland*, *22*, 54–57.

Grapes, R. H., K. Yagi, and K. Hokumura (1979), Aenigmatite, sodic pyroxene, arfvedsonite and associated minerals in syenites from Morotu, Sakhalin, *Contrib. Mineral. Petrol.*, *69*, 97–103.

Heaney, P. J., E. P. Vicenzi, L. A. Giannuzzi, and K. J. T. Livi (2001), Focused ion beam milling: A method of site-specific sample extraction for microanalysis of Earth and planetary materials, *Am. Mineral.*, *86*, 1094–1099.

Honnorez, J., and P. Kirst (1975), Petrology of rodingites from the equatorial mid-Atlantic fracture zones and their geotectonic significance, *Contrib. Mineral. Petrol.*, *49*, 233–257.

Honnorez, J., C. Laverne, H. W. Hubberten, R. Emmermann, and K. Müehlenbachs (1983), Alteration processes in layer 2 basalts from Deep Sea Drilling Project Hole 504B, Costa Rica Rift, *Initial Rep. Deep Sea Drill. Proj.*, *69*, 509–550.

Huggins, F. E., D. Virgo, and H. G. Huckenholz (1977a), Titanium-containing silicate garnets, I. The distribution of Al, Fe^{3+}, and Ti^{4+} between octaedral and tetraedral sites, *Am. Mineral.*, *62*, 475–490.

Huggins, F. E., D. Virgo, and H. G. Huckenholz (1977b), Titanium-containing silicate garnets, II. The crystal chemistry of melanite and schorlomite, *Am. Mineral.*, *62*, 646–665.

Ito, J., and C. Frondel (1967), New synthetic hydrogarnets, *Am Mineral.*, *52*, 1105–1109.

Jamtweit, B., K. V. Ragnarsdottir, and B. J. Wood (1995), On the origin of zoned grossular-andradite garnets in hydrothermal systems *Eur. J. Mineral.*, *7*, 1399–1410.

Kunitz, W. (1936), Die Rolle des Titans und Zirkonium in den gesteinsbildenden Silikaten, *Neues Jahrb. Mineral. Geol.*, *70A*, 385–466.

Kusachi, I., C. Henmi, and K. Henmi (1975), Schorlomite from Kuka, the town of Bitchu, Okayama Prefecture (in Japanese), *J. Mineral. Soc. Jpn.*, *12*, 184–191.

Laverne, C. (1983), Occurrence of melanite and aegirine-augite in Deep Sea Drilling Project Hole 504B, in *Initial Rep. Deep Sea Drill. Proj.*, *69*, 593–605.

Laverne, C. (1987), Unusual occurrence of aegirine-augite, fassãuml;te and melanite in oceanic basalts (DSDP Hole 504B), *Lithos*, *20*, 135–151.

Laverne, C. (2006), Data report: Chemical composition of unusual Ti hydrogarnets from the deepest volcanic rocks cored in ODP Hole 1256D (Leg 206) [online], *Proc. Ocean Drill. Program, Sci. Results*, *206*. (Available at http://www.odp.tamu.edu:publications/206_SR/005/005.htm.)

Lehijärvi, M. (1960), The alkaline district of Iivaara, Kuusamo, Finland, *Bull. Comm. Geol. Finland*, *185*, 62 pp.

Locock, A., W. L. Luth, G. C. Ronald, D. G. W. Smith, and M. J. M. Duke (1995), Spectroscopy of the cation distribution in the schorlomite species of garnet, *Am. Mineral.*, *80*(1–2), 27–38.

Manning, P. G., and D. C. Harris (1970), Optical absorption and electron microprobe studies of some high Ti-garnets, *Can. Mineral.*, *10*, 260–271.

Merli, M., A. Callegari, E. Cannilo, F. Caucia, M. Leona, R. Oberti, and L. Ungaretti (1995), Crystal-chemical com-

plexity in natural garnets: Structural constraints on chemical variability, *Eur. J. Mineral.*, 7, 1239–1249.

Onuki, H., M. Alasaka, T. Yoshida, and M. Nedachi (1982), Ti-rich hydroandradites from the Sanbagawa metamorphic rocks of the Shibukawa area, Central Japan, *Contrib. Mineral. Petrol.*, 80, 183–188.

Pouchou, J. L., and F. Pichoir (1985), ρ(rZ) procedure for improved quantitative microanalysis, in *Microbeam Analysis*, edited by J. T. Armstrong, p. 104, San Francisco Press, Inc., San Francisco, Calif.

Schwartz, K. B., D. A. Nolet, and R. G. Burns (1980), Mössbauer spectroscopy and crystal chemistry of natural Ti-Fe garnets, *Am. Mineral.*, 65, 142–153.

Shipboard Scientific Party (2003), Leg 206 summary, in *Proceedings of the Ocean Drilling Program*, *Initial Reports*, vol. 206, edited by D. S. Wilson et al., pp. 1–117, Ocean Drill. Program, College Station, Tex.

Switzer, G., W. G. Melson, and G. Thompson (1970), Garnet from the Mid-Atlantic Ridge near 43°N latitude, *Geol. Soc. Am. Bull.*, 81, 895–898.

Virgo, D., and H. G. Huckenholz (1974), Physical properties of synthetic titanium-bearing grandite garnets, *Carnegie Inst. Washington Year Book*, 73, 426–433.

von Eckermann, H. (1974), The chemistry and chemical properties of some minerals of the Alnö alkaline rocks, *Ark. Min. Geol.*, 5, 93–210.

Whipple, E. R. (1973), Quantitative Mössbauer spectra and chemistry of iron, Ph.D. thesis, Mass. Inst. of Technol., Cambridge.

Wilson, D. (1996), Fastest known spreading on the Miocene Cocos-Pacific plate boundary, *Geophys. Res. Lett.*, 23, 3003–3006.

Xu, W., R. Van der Voo, and R. T. Beaubouef (1997a), Alteration and dissolution of fine-grained magnetite and its effects on magnetization of the ocean floor, *Earth Planet. Sci. Lett.*, 151, 279–288.

Xu, W., D. R. Peacor, W. A. Dollase, R. Van der Voo, and R. T. Beaubouef (1997b), Transformation of titanomagnetite to titanomaghemite: A slow, two-step oxidation-ordering process in MORB, *Am. Mineral.*, 82, 1101–1110.

Zedlitz, O. (1933), Über titanhaltige Kalkeisengranate. II, *Zent. Min.*, 225–239.

Zhou, W., R. Van der Voo, and D. R. Peacor (1997), Single-domain and superparamagnetic titanomagnetite with variable Ti content in young ocean-floor basalts: No evidence for rapid alteration, *Earth Planet. Sci. Lett.*, 150, 353–362.

Zhou, W., R. Van der Voo, D. R. Peacor, and Y. Zhang (2000), Variable Ti-content and grain size of titanomagnetite as a function of cooling rate in very young MORB, *Earth Planet. Sci. Lett.*, 179, 9–20.

Zhou, W., D. R. Peacor, J. C. Alt, R. Van der Voo, and L.-S. Kao (2001), TEM study of the alteration of glass in MORB by inorganic process, *Chem. Geol.*, 174, 365–376.